Journal of Solid State Electrochemistry
https://doi.org/10.1007/s10008-025-06212-5

ORIGINAL PAPER

Impact of pH on ethanol electro-oxidation in seawater-like electrolytes: implications for ocean-based mitigation strategies

Thiago V. de B. Ferraz[1] · **Germano Tremiliosi-Filho**[1] · **Hamilton Varela**[1]

Received: 6 December 2024 / Revised: 21 January 2025 / Accepted: 22 January 2025

Abstract

This study investigates the electro-oxidation of ethanol in seawater-like electrolytes with adjusted pH, exploring its potential for CO_2 mitigation strategies. Using a polycrystalline platinum bead as a model catalyst in a conventional three-electrode cell, we demonstrate that pH adjustment significantly influences electrochemical performance, with higher oxidation current densities observed at more alkaline pH values. At pH 12, usable current densities for ethanol oxidation were achieved, attributed to the decreased surface coverage of Cl^- ions and increased ethoxy ion concentrations, consistent with observations from similar systems in the literature. However, mass transport limitations emerged at higher potential scan rates, evident from the inversion in peak current densities between pH 13 and pH 14 compared to lower scan rates. Additionally, voltammetric profiles indicated a preference for certain platinum crystallographic faces due to variations in chloride and sulfate binding strength. Notably, potential oscillations, not previously reported under such elevated Cl^- concentrations, further support these findings. Tafel analysis in the high potential region (> 1.2 V) revealed that the platinum oxide surface does not become more sensitive to ethanol oxidation with increasing pH. These insights provide an initial understanding of the main opportunities and challenges in studying and applying such systems.

Keywords Hybrid electrolysis · Chloride adsorption · Dynamic instabilities · Platinum surface · Alkaline electrolytes

Introduction

The rising concentration of atmospheric CO_2 presents substantial environmental challenges, including ocean acidification, extreme weather events, and global warming. Projections indicate that mitigating the worst effects of climate change will necessitate the removal of 10–20 Gt of CO_2 annually from 2050 until the end of the century. Among various CO_2 capture strategies, ocean-based approaches offer considerable potential due to the oceans' natural role as carbon sinks [1].

An effective strategy involves coupling electrochemical desalination systems with CO_2 capture techniques, providing the combined benefits of desalination and carbon sequestration [2, 3]. In such systems, seawater is extracted from ecologically sustainable ocean locations and subjected to pre-purification steps, such as filtration and flocculation, to remove insoluble particles and organic matter. The treated seawater is then channeled into an electrochemical cell equipped with an anion exchange membrane (AEM) and a cation exchange membrane (CEM), which separate desalinated water from a concentrated brine. This brine subsequently undergoes electrolysis, powered by renewable energy sources, driving both carbon capture and desalination. Figure 1 illustrates a generic electrochemical desalination system integrated with CO_2 capture and mineralization.

At the anode, hydrogen gas reacts in an anion-rich solution, producing an acidified stream primarily containing HCl and H_2SO_4, which can be repurposed for industrial applications. Meanwhile, at the cathode, the cation-rich aqueous solution reacts, generating hydrogen gas and an alkalized stream containing hydroxides of Na^+, K^+, Mg^{2+}, and Ca^{2+}. When exposed to atmospheric CO_2, this stream forms magnesium and calcium carbonates ($MgCO_3$ and $CaCO_3$), which can be sequestered on the ocean floor [4], used in artificial reefs [5], or applied in various industries, such as cement production [6, 7].

The remaining alkaline stream, now depleted in ions and with a slightly lower pH (though still above natural

✉ Hamilton Varela
hamiltonvarela@usp.br

[1] São Carlos Institute of Chemistry (IQSC), University of São Paulo (USP), PO Box 780, São Carlos, SP 13560-970, Brazil

Published online: 08 February 2025

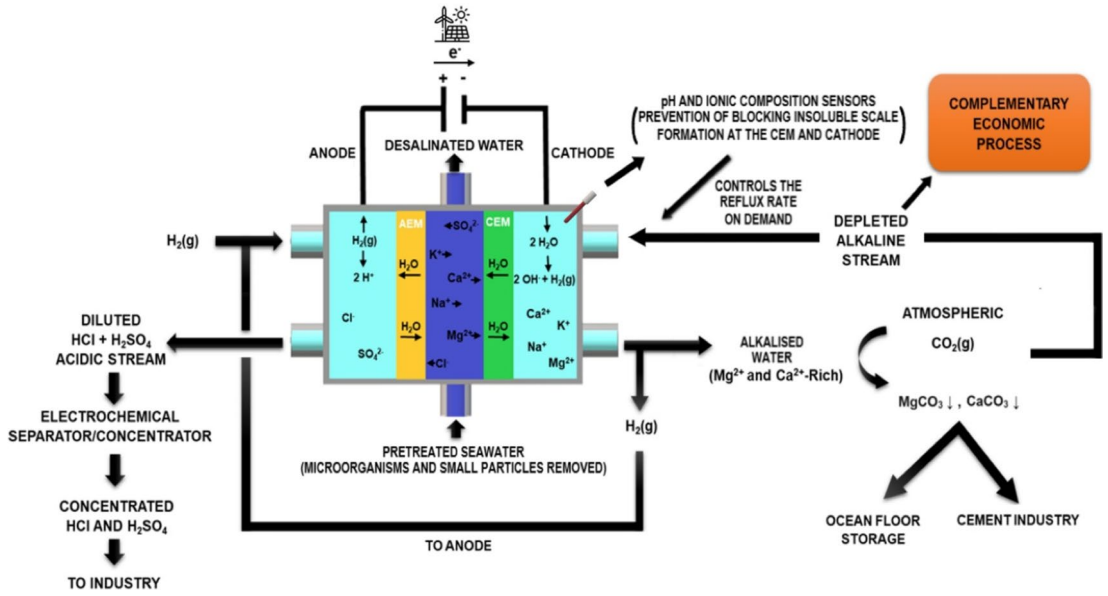

Fig. 1 Schematic representation of a generic electrochemical desalination system coupled with an atmospheric CO_2 capture and mineralization step

seawater levels of ~ 8.2), can be partially redirected to the cathodic compartment. Such recirculation helps maintain an optimal pH, thereby reducing energy consumption during water electrolysis, particularly if sensors are employed to monitor the catholyte's pH and ionic composition. These measures ensure efficient system operation and prevent scaling, which could otherwise impair performance [8].

To enhance economic feasibility, the other portion of the depleted alkaline stream could be diverted to complementary processes. This could increase the financial viability of the operation by creating opportunities for hydrogen production, CO_2 reduction into higher-value products, or both. The anodic reaction's electron supply rate determines the efficiency of these complementary processes, making the careful selection of the anodic reaction crucial [9].

Although water oxidation (WOR) is a viable anodic reaction, it produces relatively low-value products such as O_2 and H_2O_2. WOR also operates at high thermodynamic potentials and overpotentials, particularly with the catalysts most used. Other anodic reactions, such as the electro-oxidation of carbon-, nitrogen-, and sulfur-based molecules, offer economically valuable products—including pharmaceuticals [10]—and have slowly begun to be considered auxiliary reactions in hybrid seawater electrolyzers [11–13]. These reactions operate at lower thermodynamic potentials and overpotentials than WOR, making them promising alternatives. Additionally, they broaden the range of valuable products that can be generated, thereby increasing the system's economic viability. Figure 2 illustrates some of these alternative anodic reactions, highlighting their potential to produce a wider array of valuable products compared to water oxidation.

To maximize economic efficiency, it would be advantageous to construct facilities employing these alternative anodic reactions in coastal areas near regions where these compounds are already produced, stored, or transported. For instance, locating such installations near seaports would facilitate logistics and reduce the costs associated with transporting materials and the solutions containing the products generated to electrochemical processing, separation, and wastewater treatment plants.

Among the alternative anodic processes, ethanol electrooxidation stands out as a particularly attractive option. Ethanol, a biomass-derived organic molecule, has smaller oxidation overpotentials compared to water ($E^{o}_{(CO_2/C_2H_5OH)}$ = 0.08 V vs. SHE) [14], making it an efficient candidate for electrochemical processes. Ethanol is also easier to store and transport, with a volumetric energy density of 6.7 kWh/L compared to 1.3 kWh/L for hydrogen at 700 bar [15, 16]. Moreover, ethanol oxidation yields valuable by-products, such as acetaldehyde and acetic acid, enhancing its economic appeal [17].

Ethanol's role in seawater-based systems has been explored in various related applications, such as biofuel production and desalination, where it can help reduce the energy costs associated with traditional methods [18–22]. By leveraging its chemical properties in these contexts, ethanol becomes a key component in enhancing the economic feasibility of seawater desalination systems coupled with CO_2 capture. Its unique interaction with seawater offers

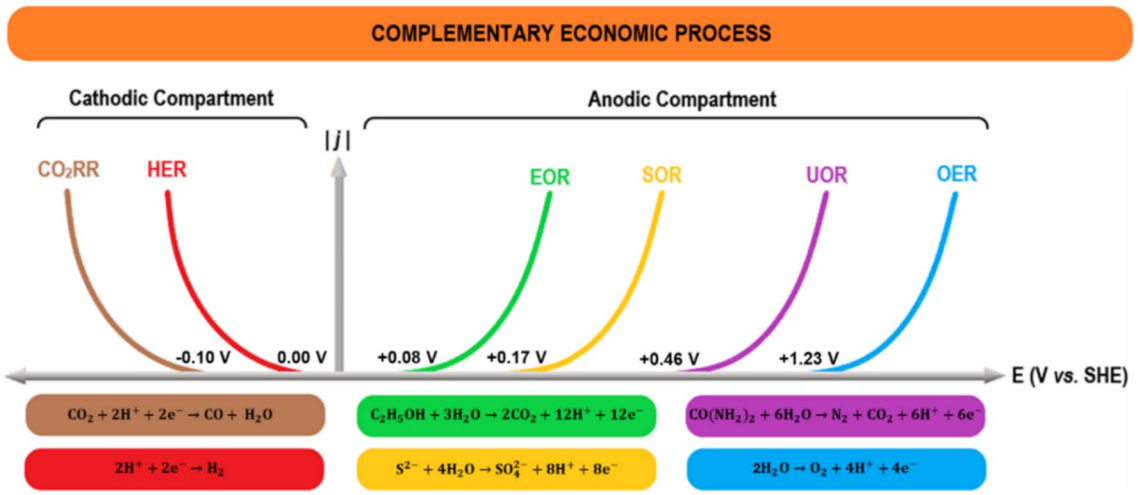

Fig. 2 Illustrative j–E curves comparing the thermodynamic equilibrium potentials for various reactions of small organic molecules that have the potential to assist in complementary economic processes involving seawater electrolysis. From left to right: CO_2RR, carbon dioxide reduction reaction; HER, hydrogen evolution reaction; EOR, ethanol oxidation reaction; SOR, sulfide oxidation reaction; UOR, urea oxidation reaction, OER, oxygen evolution reaction. Based on [12, 13]

opportunities for improved reaction selectivity and yield, particularly in systems where chloride ions are abundant.

Typically, a sample of water from a random point in the ocean will exhibit a chloride (Cl^-) concentration of around 0.5 M [23]. In the 1930s, Frumkin and collaborators observed that halide anions tend to strongly adsorb onto noble transition metal electrodes in acidic aqueous solutions—findings later expanded by Breiter and Gilman in the 1960s, and Horányi and Bagotzky in the 1970s [24–27]. In 1981, Novak and Conway recognized a fundamental difference between Br^-/I^- and Cl^- ions in their adsorption behavior—while the former follows a Langmuir-type isotherm, chloride ions adhere to a linear logarithmic isotherm [28].

This aspect directly influences the response of the electrode/electrolyte interface in the presence of neutral species in the medium. For example, Sobkowski et al. [29] observed that bromide and iodide concentrations as low as 10^{-5} M can significantly inhibit methanol oxidation on a polycrystalline platinum electrode in acidic conditions, whereas a Cl^- concentration of approximately 10^{-3} M is required to produce a similar effect—largely due to the relative ease with which alcohol molecules displace adsorbed water molecules and chloride ions.

For ethanol, the literature on its electro-oxidation at moderate potentials in the presence of Cl^- anions is somewhat limited. Notably, two papers from the 1980s by Snell and Keenan [30, 31] focused on platinum in both neutral and acidic solutions, drawing conclusions similar to those found for methanol decades earlier [32–35]. Additionally, a 2016 paper by Kumar et al. [36] investigated this process on a palladium electrode in alkaline media. Interestingly, even at a NaCl concentration as high as 0.1 M and a pH of 13, the anodic current observed for this system was significantly higher than that for the same reaction carried out with similar alcohol concentrations but only trace amounts of chloride ions in a low pH medium.

A comprehensive phenomenological model, applicable to observations of this kind, was developed in a study by Attard [37], which argued that increasing the pH of the medium shifts the potential of zero charge to higher values due to a greater surface concentration of negative charges from adsorbed OH^- anions. This, in turn, decreases the surface coverage of other strongly binding negatively charged species, such as chloride anions. The implications of this effect have been explored with some success in the adjacent field of seawater electrolysis [38–41], where natural waters are alkalinized to increase the selectivity of the anodic process towards water oxidation rather than the typically undesired chloride oxidation reactions (COR). However, there has not yet been a systematic study focused on evaluating how the transition from neutral to high pH conditions affects the oxidation of organic species like ethanol in a chloride-rich medium.

Building on the preceding points, we present here an initial assessment of the fundamental aspects of ethanol electro-oxidation in seawater, employing a simplified seawater electrolytic matrix and a model polycrystalline platinum electrode to identify and explore key factors influencing this process. In doing so, we aim to provide insights while also laying the groundwork for further research into the potential benefits and challenges of integrating ethanol into electrochemical CO_2 capture and desalination systems coupled with hybrid seawater electrolysis.

Experimental

Reagent and solution preparation

All solutions were prepared using analytical grade reagents (≥ 99%)—NaCl (Panreac), Na_2SO_4 (Sigma-Aldrich), NaOH (Sigma-Aldrich), H_2SO_4 96.5% (Exodo Cientifica), absolute ethanol (Supelco)—and ultrapure deionized water (Millipore, 18.2 MΩ cm). The seawater-mimicking electrolyte was a simplified version of the ionic matrix suggested by the international standard ASTM D1141-98, consisting of 0.5 M NaCl and 0.05 M Na_2SO_4, with the ethanol concentration maintained at 1 M in all relevant experiments.

Experimental setup configuration

The electrochemical measurements were conducted in a conventional three-electrode cell. The working and counter electrodes were polycrystalline platinum—a spherical bead with a 1.05 mm radius and a large surface area coil, respectively—while the reference electrode was a reversible hydrogen electrode (RHE) filled with the same support electrolyte used in each experiment. Unless otherwise stated, all measurements and equations reported and discussed are referenced to the RHE.

Reference electrode calibration

For solutions with pH lower than 12, the RHE electrode displays pseudo-reference behavior after stabilization. It was calibrated with respect to the hydrogen evolution reaction (HER, $E^{o} = 0.00$ V vs. RHE) before and after the addition of alcohol.

Equipment used

A potentiostat/galvanostat (Autolab PGSTAT302N) with the Nova interface (version 2.1.7) was used for the measurements.

Glassware cleaning and electrode conditioning

Before each set of measurements, the glassware was cleaned with potassium permanganate and diluted piranha solutions according to procedures described elsewhere [42]. Both platinum electrodes were flame annealed for a few seconds and then inserted into the argon-deaerated system maintained at 25 °C. The working electrode surface was electrochemically conditioned prior to each measurement to ensure reproducibility (Fig. 3). This procedure was based on Gilman [43]. All experimental data presented and discussed in the following sections were selected from reproducible replicates to represent each condition.

Determination of electrochemically active surface area

The electrochemically active surface area (ECSA) of the pc-Pt bead was determined for the purpose of normalization by integrating the charge from the hydrogen desorption region of voltammograms obtained in a 0.5 M H_2SO_4 solution at 50 mV s^{-1}. The calculation followed a standard procedure based on cyclic voltammetry in the well-characterized hydrogen adsorption/desorption region of the platinum surface [44].

Cyclic voltammetry: Cyclic voltammetry scans were conducted within the potential range corresponding to hydrogen adsorption/desorption on the platinum surface.

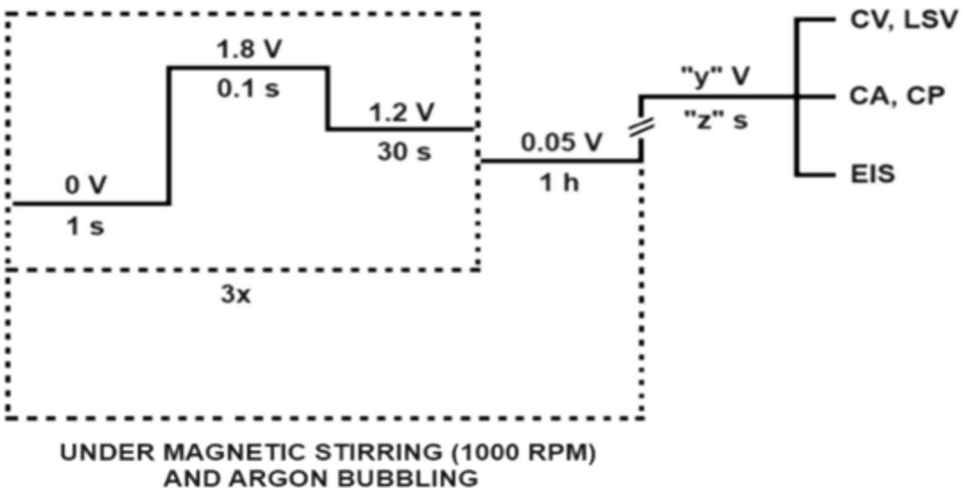

Fig. 3 Diagrammatic representation of the steps involved in the electrochemical pre-conditioning of the electrode before each measurement, where "*y*" corresponds to the specific values of fixed potential applied at the beginning of each procedure (i.e., cyclic voltammetry (CV), linear sweep voltammetry (LSV), chronoamperometry (CA), chronopotentiometry (CP), and electrochemical impedance spectroscopy (EIS)) and "*z*" to the duration of the application

Charge integration: The charge (Q_H) associated with the hydrogen adsorption/desorption peaks was integrated. This charge is directly proportional to the available electroactive sites for hydrogen adsorption on the electrode.
ECSA calculation: The electrochemically active surface area was then calculated using the following equation:

$$\mathrm{ECSA} = \frac{Q_H}{0.210\ \mathrm{mC\ cm^{-2}}} \quad (1)$$

where Q_H represents the charge for hydrogen adsorption/desorption, and 0.210 mC cm^{-2} is the standard charge density corresponding to a monolayer of hydrogen on polycrystalline platinum [45].

Multiple measurements were performed to validate the reproducibility and accuracy of the ECSA values, resulting in a roughness factor of 1.041 ± 0.037 for the electrode used in subsequent experiments. Further details on the reasoning behind the choice of this method can be found in Section S.1 of the Online Resource.

Determination of the cell's uncompensated resistance

The uncompensated resistance (R_u) of the electrochemical system was estimated before each set of voltammetric measurements using electrochemical impedance spectroscopy. Data were acquired at the open-circuit potential (OCP), and R_u was determined from the *x*-axis intercept (real impedance, Z_{real}) in the high-frequency region (> 10 kHz) of the Nyquist plot. The corresponding potential drop resulting from this resistance (*iR* drop) was corrected during data analysis to ensure accuracy in the reported voltammetric results and consistency between measurements. The R_u values were approximately 15 Ω for systems with pure electrolyte solutions and around 20 Ω for solutions containing 1 M ethanol.

Results and discussion

The electro-oxidation of ethanol is known to proceed through distinct mechanistic steps, depending on whether the catalytic site interacting with the alcohol molecule is part of a metallic surface or an oxide layer [46]. For clarity, the discussion has been divided into three topics—two based on the potential windows where each process occurs and one for a more comprehensive analysis of the findings. These are presented as follows:

Low to moderate potential region (0.05–1.20 V)

It is widely accepted that ethanol electro-oxidation at low to moderate potentials over metallic platinum catalysts proceeds through successive oxidative dehydrogenation steps (Eq. 2). The products formed are typically the most stable solution species, produced via the reaction of adsorbed organic fragments with neighboring Pt-OH groups, following a Langmuir-Hinshelwood mechanism. These species mainly include acetaldehyde, acetic acid, and carbon dioxide [47].

$$[X]_{ads} + \mathrm{Pt} \rightarrow \mathrm{Pt} - X^* + \mathrm{H^+} + \mathrm{e^-} \quad (2)$$

In which $X/X^* = CH_3CH_2OH$, CH_3CHOH, CH_3COH, CH_3CO, and CO (in this sequence of reactions).

While the surface-inhibiting effects of chloride ions at low pH (and their attenuation in strongly alkaline media) have been reported to some extent over various noble metals (as discussed in the introduction), a systematic study addressing how pH variation affects the specific kinetic aspects of this process is still lacking. Therefore, the first step of this investigation involved obtaining electrochemical profiles for the system across a wide range of pH values (8 to 14) in the potential range of 0.05 to 1.20 V. The cyclic voltammograms recorded for the solutions with and without 1 M ethanol are shown in Fig. 4.

An inspection of the electrochemical behavior of the polycrystalline platinum (pc-Pt) electrode in the pure support electrolyte shows that at pH 8, most processes related to platinum oxide formation/reduction and hydrogen adsorption/desorption are inhibited. This is attributed to the strong adsorption of chloride ions [24]. As the pH increases to 14, the inhibition effect becomes less pronounced, likely due to a reduction in Cl^- surface coverage, as the potential of zero charge (PZC) shifts to higher values due to the increasing concentration of negatively charged OH^- groups on the electrode surface [37].

Interestingly, the evolution of the voltammetric profile of polycrystalline platinum with increasing pH differs markedly from what has been reported in studies using supporting electrolytes with more conventional anions (e.g., ClO_4^-, SO_4^{2--}, and Pi—inorganic phosphate ions) [48–51]. This divergence likely arises from the strong specific adsorption of chloride ions, which alters the surface dynamics compared to systems where only perchlorate or sulfate ions are present.

A closer inspection also suggests a trend towards the selective exposure of certain crystallographic faces of polycrystalline platinum as pH increases. Although some asymmetries are observed between the cathodic and anodic scans compared to known profiles of respective single-crystal highly polarizable electrodes [52, 53], patterns emerge. At pH 8, the shape and current density of the H adsorption region resemble Pt(110). With increasing OH^- concentrations, features of Pt(100) emerge at pH 9 and 10,

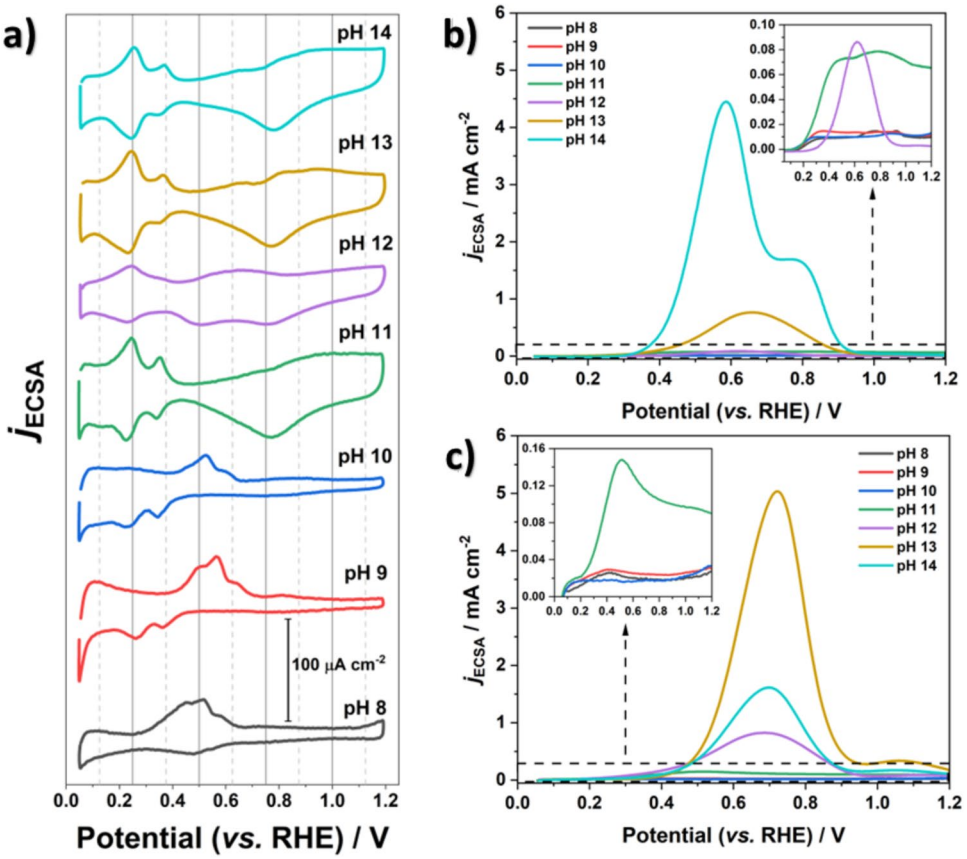

Fig. 4 **a** Cyclic voltammograms of the supporting electrolyte for different pH values in the range of 8–14 recorded at 50 mV s^{-1} and voltammetric profiles for the solutions containing 1 M ethanol recorded between 0.05 and 1.20 V (vs. RHE) at **b** 1 mV s^{-1} and **c** 50 mV s^{-1}. Support electrolyte comprised of 0.5 M NaCl and 0.05 M Na_2SO_4

and for pH 11 and above, the surface behavior aligns with that of polycrystalline platinum in alkaline media [54, 55].

It is well documented that the adsorption strength of anions on platinum varies with atomic coordination, following the order {111} > {100} > {110} [56]. This suggests that chloride ions preferentially adsorb at certain sites due to significant differences in binding energies. However, as the pH increases, electrostatic repulsion is expected to build up within the electrode/electrolyte interface due to the increasing concentration of negatively charged OH^- ions. In principle, the heterogeneous 2D surface occupancy would lead to imbalances in repulsive forces between neighboring chloride ions, eventually leading to a reorganization of the adsorbed layer as repulsive forces approach the species' binding energy [57, 58]. This is supported by the behavior observed at pH 12, where electrochemical features of the pc-Pt surface are briefly subdued compared to pH 11, before re-emerging at pH 13.

From another perspective, the alleviating effect of increasing the medium pH on the surface inhibition promoted by chloride ions also has a noticeable impact on the voltammetric profiles of the system in the presence of 1 M ethanol. As can be seen in Fig. 4b, for pH values up to 10, there are only weak signs of the fragmentation of ethanol and water molecules on the platinum surface at around 0.30 V and 0.95 V, respectively, without any indication of reactions between the formed organic and oxygenated groups—characteristic of the EOR processes. This suggests the difficulty ethanol molecules face in adsorbing and reacting with the platinum electrode surface in appreciable amounts due to the high Cl^- surface coverage.

As the pH increases to 11, there is a sudden surge in the system's current baseline, accompanied by the appearance of two distinct peaks attributed to the preferential fragmentation and partial oxidation of the negatively charged ethoxy species, rather than ethanol, to acetaldehyde. Ethanol has a pK_a of approximately 15, and a medium with a pH of 11 corresponds to the lower limit where a non-negligible concentration of ethoxy species exists [59]. Additionally, the fact that the observed current does not rapidly diminish within the potential window considered could be associated with increased formation of polarized organic fragments (pseudocapacitive contribution) that are not readily removed from the electrode surface, likely due to the insufficient formation of neighboring Pt-OH groups—which would indicate a higher affinity of the platinum metallic sites for ethanol rather than water/hydroxide at pH ≤ 11.

As the pH increases to 12 and 13, the system exhibits a consistent rise in the current of a well-defined oxidation process, consistent with the increase in OH^- concentration

and its previously mentioned positive effects on ethoxy and Pt-OH group concentrations. Finally, at pH 14, a similar enhancement in current density is observed; however, the process appears to deconvolute into two peaks: a more intense one centered at 0.58 V and a less pronounced one at 0.79 V—an observation consistent with reports stating that, in the absence of strongly adsorbing anions, the C_1-pathway, in which the carbon-carbon bonds in ethanol and acetaldehyde are broken (leading to the formation of CO_2), is favored to a minor extent [60].

The scan rate of the voltammetric measurements significantly affects the system's response across different pH values, as seen in Fig. 4b (1 mV s^{-1}) and c (50 mV s^{-1}). Most of the trends discussed above remain visible at faster scan rates, though some deviations emerge. One noticeable difference is the reversal of the EOR intensity at pH 13 and 14 for the faster scan.

There are two main hypotheses that could explain the higher current density observed at pH 13 under these conditions. First, the rapid scan rate may prevent the dissipation of the pH gradient formed due to reactions like those expressed in Eq. 2, resulting in an effective interfacial pH significantly lower than that of the bulk solution [61]. Second, at high OH^- concentrations, hydroxide ions may act as surface-inhibiting species toward ethanol due to their large difference in diffusion coefficients—an effect more readily revealed at faster scan rates where mass transport limitations become more pronounced [62].

Given the remarkable sensitivity of their response to the immediate interface conditions during the catalytic process, dynamic instabilities were evaluated in the system in the presence of ethanol at the pH values considered. The collected data are shown in Fig. 5.

The galvanodynamic curves obtained for pH values from 8 to 14 (Fig. 5a) show that: (*i*) for pH 8 to 10, the potential rapidly increases into the oxygen evolution reaction/chloride oxidation reaction region with little variation in current densities; (*ii*) for pH 11 and 12, there is a considerable shift in the profile for larger current density values before the sharp rise in potential; and (*iii*) for pH 13 and 14, bistable behavior (coexistence of two stable equilibrium states) is observed in distinct and non-overlapping current density windows, with pH 13 displaying a considerably larger region of potential oscillation compared to pH 14.

Such oscillatory behavior aligns with the phenomenon of dynamic instabilities in heterogeneous catalysis, systematically and extensively investigated by Gerhard Ertl and his collaborators [63]. Although Ertl's early research primarily focused on gas-phase reactions on metal surfaces, particularly platinum, his insights into molecular adsorption dynamics (e.g., CO and O_2) laid the groundwork for later addressing instabilities in electrochemical systems involving more complex molecules, such as formic acid and methanol [64–66]. The coupling of a surface poisoning process with a slower, potential-dependent oxidation reaction—described in the 'hidden negative impedance' model derived from his ideas and further developed notably by Eiswirth, Krischer, Koper, and Strasser [67–69]—provides a valuable framework for interpreting the oscillations observed here. This model illustrates how surface poisoning by intermediates and the regeneration of active sites at different rates can result in oscillatory behavior [70]. In our system, a similar interaction between chloride adsorption and subsequent oxidation processes may underlie the potential oscillations observed at higher pH values.

Despite the existence of a few studies addressing dynamic instabilities during the electro-oxidation of carbon-based compounds on platinum in the presence of Cl^- ions [27, 71–73], direct comparisons with the present findings should be approached cautiously. None of the previous studies was conducted under such high chloride concentrations and alkaline conditions. For instance, the widening of the current density window where potential instabilities were observed for methanol oxidation, as reported by Fiori et al. [74], initially appears consistent with the reduction in anion surface coverage as pH increases. However, their experiments in acidic conditions do not account for the mass transport limitations inherent to highly alkaline solutions [62].

To better understand the processes occurring during the observed potential oscillations, galvanostatic time series were obtained for pH 13 and 14. Since the instabilities occur in distinct and non-overlapping current density windows, the current densities chosen for comparison were normalized using a method proposed by Varela and co-workers [75]:

$$j_N = \frac{j_{osc} - j_{osc,i}}{j_{osc,f} - j_{osc,i}} \tag{3}$$

where j_{osc} is the applied current density, and $j_{osc,i}$ and $j_{osc,f}$ are the initial and final current densities that define the observed oscillatory potential regions, respectively.

Despite the more than 3-fold difference between any possible chosen j_N values associated with the pH 13 and 14 cases, all of them felt within narrow potential windows corresponding to the immediate descending branch following the peak of their respective voltammetric oxidation process waves (the single one from pH 13 and the second one from pH 14— Fig. 5b and c). The results corresponding to the current density values associated with the midpoint of each oscillation window ($j_{0.5}$) are shown in Fig. 5d and e.

The shape, amplitude, and evolutionary trend of the potential oscillations observed for these time series are essentially the same, with the most significant variations associated with the period of the oscillations. Regarding the last point, while the average oscillation period ($\overline{\tau}$) does not contain enough information by itself to completely

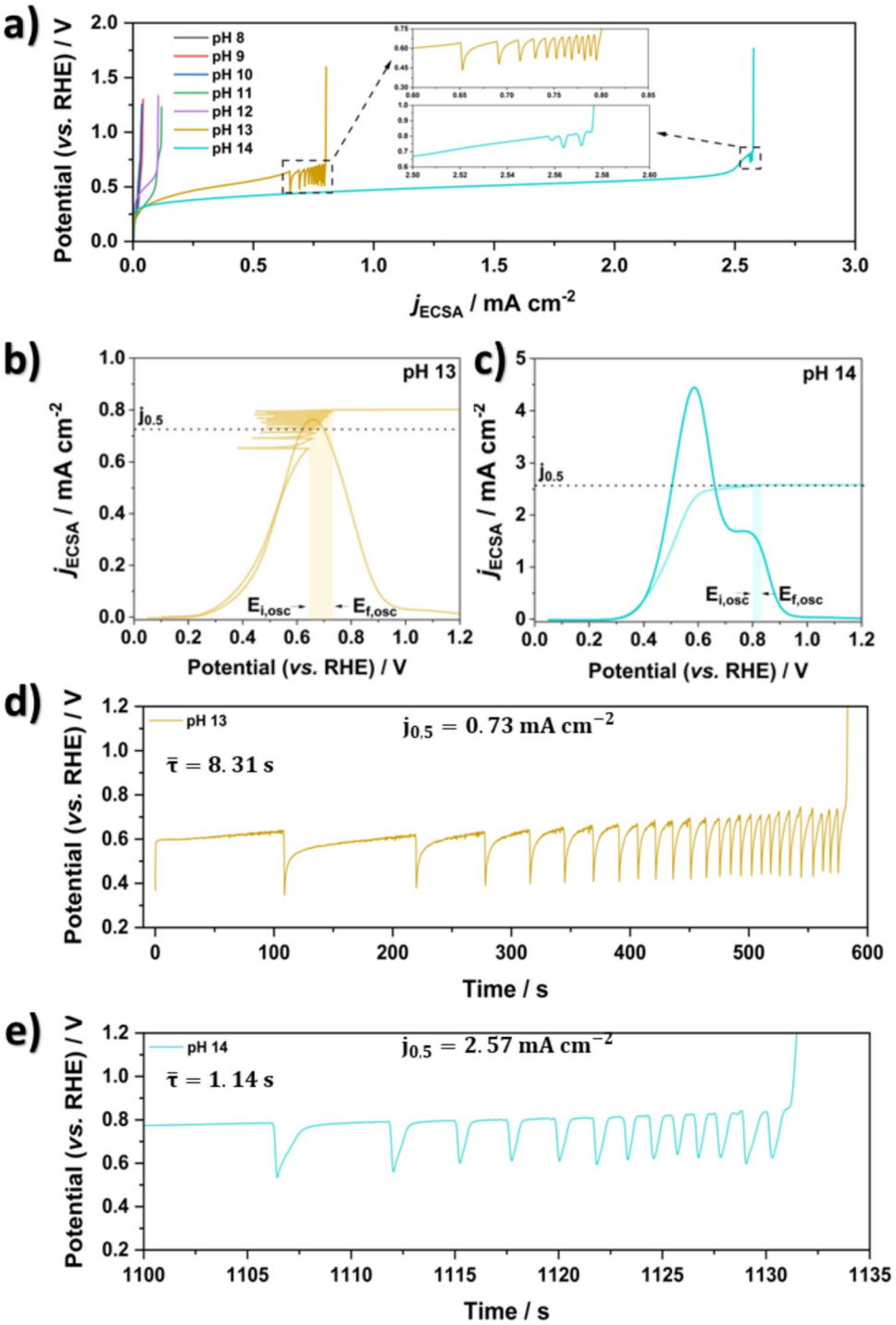

Fig. 5 **a** Galvanodynamic curves obtained at 100 nA s^{-1} (777 ± 48 nA s^{-1} cm^{-2}) for different pH values ranging from 8 to 14 during ethanol electro-oxidation under conditions identical to those presented in Fig. 4b. Inset: close-up view of the potential oscillations. Overlay of the galvanodynamic curves and corresponding voltammetric profiles (with 100% *iR* drop correction) for **b** pH 13 and **c** pH 14, where $E_{i,osc}$ and $E_{f,osc}$ represent the potential values at which oscillatory behavior begins and ends, respectively. Galvanostatic time series for the samples at **d** pH 13 and **e** pH 14, with fixed current values corresponding to normalization by $j_{0.5}$

characterize the dynamic behavior of the system, it still provides some useful insights.

For instance, Körös's [76] approach treats oscillations as a pseudo-monomolecular reaction, where the reciprocal of the oscillation period is analogous to a first-order rate constant. Combined with the Arrhenius equation, this implies that $\bar{\tau}$ would be directly proportional to the activation energy (E_a) of the overall process [75] and that E_a(pH 13) > E_a(pH 14)—suggesting thus higher activation energy at pH 13 [77].

Moreover, this observation intersects with Temkin's rule [78], which posits that the average oscillation period can represent the relaxation time of a group of competing surface reactions as they approach a steady state (which is never fully achieved during dynamic instabilities [79]).

Upon closer inspection of the instability time series, it is evident that at lower maximum potential values (corresponding to the peak of the poisoning process), the oscillations exhibit longer periods and plateau-like profiles. These suggest the presence of more weakly bonded species, such as carboxylates (e.g., acetate from acetaldehyde oxidation), on the electrode surface [80–82]. As the maximum potential increases, the oscillation period shortens and transitions to a sawtooth-like shape, indicating the poisoning and cleaning of the electrode surface by strongly adsorbed species, such as Pt-CO, through a Langmuir-Hinshelwood-type mechanism involving Pt-OH groups and CO_2 production [60, 82].

Interestingly, another noteworthy pattern emerges when the oscillation profiles observed here are compared to those reported in the literature for the ethanol oxidation reaction on various single-crystal platinum surfaces [82]. The time series presented in this study closely resemble those recorded for Pt(100) and Pt(110) electrodes in NaOH electrolyte with ethanol, both in terms of shape and trend.

Considering the observations by Previdello et al. [83], which suggest that the specific characteristics of these time series—such as shape, amplitude, and period—are highly sensitive to the identity of the crystallographic faces and defects present on the platinum electrode surface, this provides compelling evidence that selective exposure of these planes, influenced by pH and chloride ion interactions, plays a pivotal role in defining the observed oscillatory behavior. Consequently, such selective plane exposure may significantly influence the overall electrochemical performance of the electrode during the oxidation of organic molecules, in a manner similar to that observed for single-crystal platinum surfaces and preferentially domain-ordered nanoparticles [52, 53, 84].

However, this inference contrasts with the earlier observation that the cyclic voltammograms for the platinum electrode in the pure electrolyte solution (Fig. 4a) exhibit a polycrystalline profile at pH 13 and 14. This apparent contradiction can be reconciled by considering the effect of introducing a more apolar organic compound into a polar medium containing dissolved salts. Such an addition can not only induce the precipitation of these salts by disrupting the solvation structure of their constituent ions, but also increase the concentration of these ions near the electrode/solution interface by affecting the dielectric constant of the medium and, consequently, shifting their adsorption/desorption equilibrium (reflected in their degree of coverage)—provided that, from an energetic perspective, the stabilization offered by the easier adsorption of ions with a looser solvation sphere on the electrode is greater than that gained by the formation of ionic pairs [85–87]. As a result, this may counteract the reduction in chloride ion affinity for platinum sites induced by the higher OH^- concentration, thereby influencing the expected electrode response.

Altogether, the analysis of dynamic instabilities reinforces the inferences made throughout this discussion. However, further investigation is required to fully understand the mechanistic behavior of the system within this potential window.

High potential region (> 1.20 V)

Although current densities in the range of 1–10 mA cm^{-2} achieved for the EOR at approximately 0.7 V are attractive from an energetic perspective, the economic feasibility of applying this process depends heavily on the system's configuration and operational parameters (e.g., temperature and flow rate of the solution). Without further adjustments to the electrolyte or catalyst composition, achieving higher current densities would require increasing the applied potential.

In this context, reducing the potential bias required for a given current density, facilitated by the presence of ethanol compared to the higher overpotentials of water or chloride oxidation reactions, is of considerable interest. Nevertheless, the mechanistic considerations at play differ fundamentally from those discussed earlier.

Firstly, under the alkaline pH values considered (see Section S.2 of the Online Resource for mechanistic considerations under acidic and neutral conditions), the upper potential limit signifies a substantial change in the chemical identity and reactivity of the platinum surface. In the range of 0.95 to 1.15 V, superficial Pt-OH groups are converted to Pt-O species, which are further oxidized to a PtO_2 phase above 1.15 V [88]. These Pt-O units then become the preferred catalytic sites for the EOR, replacing the metallic Pt atoms (Eqs. 4–7, inspired by [89]).

$$Pt - O + OH^- \rightarrow Pt - OOH + e^- \quad (4)$$

$$Pt - OOH + OH^- \rightarrow Pt + O_2 + H_2O + e^- \quad (5)$$

$$Pt + OH^- \rightarrow Pt - OH + e^- \quad (6)$$

$$Pt - OH + OH^- \rightarrow Pt - O + H_2O + e^- \quad (7)$$

While incomplete oxidation products such as ethyl acetate and acetone are observed with other transition metal oxides (in various heterogeneous reforming procedures) [90, 91], platinum oxide typically yields only acetaldehyde and acetic acid [88, 92–94].

However, the expected selectivity of the oxidation process at potentials > 1.20 V is complex. In the given electrolyte, a wide potential window exists where both the oxygen evolution reaction ($E^o_{O_2/H_2O} = E^o_{O_2/OH^-} = 1.229$ V—Equations S16 and S27) and chloride oxidation reactions ($E^o_{Cl_2/Cl^-} = 1.378$ V; $E^o_{HClO/Cl^-} = 1.454$ V; $E^o_{ClO^-/Cl^-} = 1.673$ V—Equa-

tions S6, S11, and S22) are thermodynamically favorable [40, 95, 96].

The challenge is exacerbated by the fact that all these reactions share the Pt-O groups as catalytic sites, including the EOR (Eqs. 8–12, based on [88, 94, 97, 98]) and the COR (Eqs. 13 and 14, inspired by [99] for solutions with pH > 7.54).

$$Pt - O + CH_3CH_2OH \rightarrow Pt - (OCH_2CH_3) + H^+ + e^- \quad (8)$$

$$Pt - \left(OCH_2CH_3\right) \rightarrow Pt + CH_3CHO + H^+ + e^- \quad (9)$$

$$Pt - O + CH_3CHO \rightarrow Pt - (OOCCH_3) + H^+ + e^- \quad (10)$$

$$Pt + OH^- \rightarrow Pt - OH + e^- \quad (11)$$

$$Pt - \left(OOCCH_3\right) + Pt - OH \rightarrow Pt + Pt - O + CH_3COOH \quad (12)$$

$$Pt - O + Cl^- \rightarrow Pt - OCl + e^- \quad (13)$$

$$Pt - OCl + OH^- \rightarrow Pt - OH + ClO^- \quad (14)$$

To assess the impact of pH on the influence of these reactions, polarization measurements were conducted under stationary conditions at a slow scan rate, with the results presented in Fig. 6.

The LSVs for the system containing only the support electrolyte (Fig. 6a) reveal two distinct sets of pH conditions with consistent features. For $8 \leq pH \leq 11$, the profiles are similar in shape, tightly grouped, with an average shift of + 0.03 V per added pH unit and a sharp increase in current densities—only + 0.06 V is required to raise the current densities from 0.5 to 5 mA cm^{-2} across these conditions.

For $pH \geq 12$, the polarization curves begin to show an increase in current density at considerably lower onset potential values (around 1.55 V) compared to those observed for $pH \leq 11$, albeit at a slower rate. An overpotential of + 0.467 V is required to reach $j_{5\ mA\ cm^{-2}}$ at pH 12 compared to pH 11, with values of + 0.810 V, + 0.710 V, and + 0.380 V needed to increase from $j_{0.5}$ to $j_{5\ mA\ cm^{-2}}$ for pH 12, 13, and 14, respectively (Fig. 6c).

While these findings may seem to contradict the thermodynamically predicted preference for OER over COR, they are consistent with studies showing that COR, a two-electron process, is kinetically more favorable than OER, a four-electron process [40]. However, neither kinetic preference nor thermodynamic favorability alone determines selectivity under specific experimental conditions.

A useful descriptor for the observed selectivity was proposed by Exner et al. [100]. They suggested that when the rate-determining step (RDS) involves the formation of Pt-OOH, water (H_2O/OH^-) and chloride (Cl^-) ions compete for adsorption at the shared catalytic Pt-O site. The Gibbs free energy of the Pt-OCl intermediate ($\Delta G^{\ddagger}$(Pt-OCl)) is always lower than that of Pt-OOH ($\Delta G^{\ddagger}$(Pt-OOH)), meaning that COR is always kinetically favored over OER at lower potentials. Thus, the difference in activation energies ($\Delta G^{\ddagger}$(Pt-OOH) − $\Delta G^{\ddagger}$(Pt-OCl)) serves as a key measure of the system's selectivity between COR and OER [101].

For pH values ≤ 11, the reaction kinetics appear largely unaffected by the increase in OH^- concentration, suggesting that the RDS is not sensitive to OH^- concentration or its influence on Cl^- adsorption. This implies that neither the step in Eq. 13 nor the alternative in Eq. 14 serves as the RDS.

Additionally, the onset potentials for the observed processes are lower than the thermodynamically predicted values for chloride oxidation to hypochlorite ions. However, they align with the expected values for hypochlorous acid (HClO) formation at pH levels below 7.54—relative to the pKa for $HClO/ClO^-$ interconversion (Equation S29). This is further supported by the observed potential shift of approximately + 0.03 V per pH unit, as anticipated for the reaction in Equation S11.

These findings indicate that the effective pH at the electrode/solution interface during the process is significantly lower than the nominal bulk solution pH. This conclusion is consistent with previous studies, which report that, particularly in unbuffered solutions, oxidation at the metal electrode surface can create a localized pH gradient lower than that of the bulk [55, 61, 102]. This effect results from the consumption of OH^- (Eqs. 4–7) or the generation of H^+ (primarily from Equations S1, S12–S14). Consequently, chloride oxidation to hypochlorous acid, rather than hypochlorite ions, seems to dominate in solutions with nominal pH values ≤ 11.

The Tafel slopes from the LSV curves (Fig. 6e) support these conclusions. For pH values ≤ 10, the coefficients are around 40 mV dec^{-1}, aligning with the theoretical value expected for COR, where the final chemical step (Equation S9) is independent of $[OH^-]$ and Cl^- adsorption strength [99]. At pH 11, there is a sharp decrease in slope to 18 mV dec^{-1} (indicating a shift in the RDS) and the appearance of another linear region at lower current densities, with an angular coefficient close to 100 mV dec^{-1}, consistent with values observed for OER on similar electrodes [103].

For $pH \geq 12$, the Tafel slope values for lower current densities tend to decrease as pH increases, despite an initial inversion at pH 12 (potentially linked to the anionic adlayer phase transition discussed earlier). This suggests a kinetic favoring of the reaction at higher $[OH^-]$ levels. A similar trend is observed in the additional Tafel region at higher current densities, where elevated coefficients are likely due to mass transport limitations during oxidation [103].

While it is common to attribute the presence of voltammetric anomalies—such as the current density plateaus

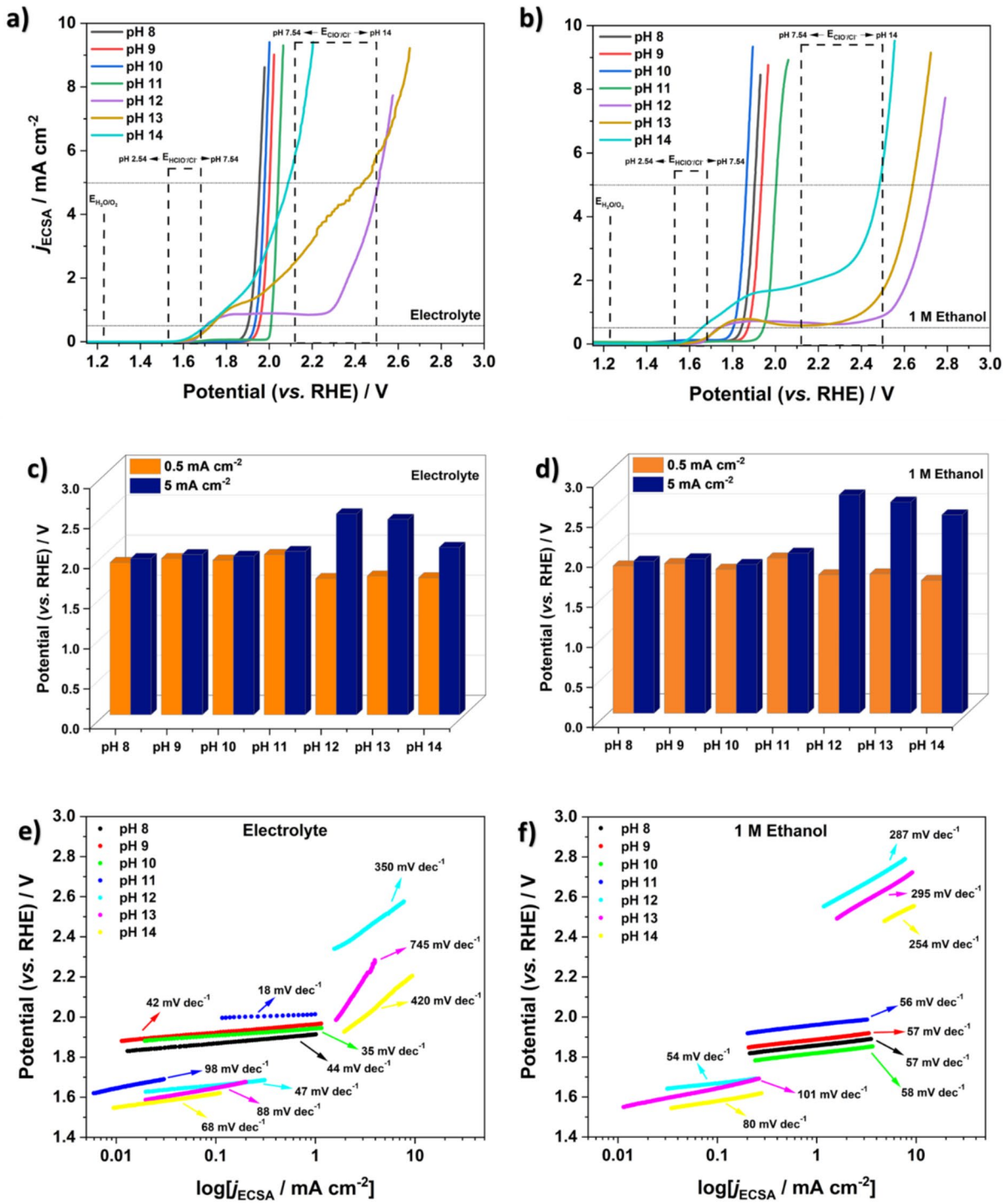

Fig. 6 **a**, **b** Linear sweep voltammograms recorded for seawater-like solutions at various pH values in the potential window between 0.05 and 1.20 V and with a scan rate of 1 mV s^{-1} (95% *iR* drop correction). **c**, **d** Bar graphs depicting the relationship between pH values and the potential required to achieve current densities of 0.5 mA cm^{-2} (orange bars) and 5 mA cm^{-2} (blue bars). **e**, **f** Tafel plots extracted from the LSV data (100% *iR* drop correction). The images on the left side (**a**, **c**, and **e**) pertain to the system without alcohol, while the ones on the right side are for the system with 1 M ethanol

observed just below 1 mA cm^{-2}—to mass transport limitations (e.g., bubble formation, typically mitigated by electrode rotation) [104, 105], studies by Shinagawa et al. [106] and Fujita et al. [101], using rotating ring-disk electrodes to examine chloride-rich systems at various pH levels, reached a different conclusion for this particular case. They suggest that the current density plateaus result from a transition at pH 12, where OH^- ions replace H_2O as the primary reactants in the OER. Their findings also suggest that COR competes with OER when H_2O is the primary reactant, but not when OH^- becomes the dominant species.

Interestingly, the addition of 1 M ethanol did not significantly alter the voltammetric profile shape, average potential shifts with increasing pH, or Tafel kinetic parameters. This indicates that the COR and OER turnovers on the catalyst surface dominate over the EOR within the pH range considered. However, some ethanol molecules do interact with the platinum oxide surface, as seen by the larger potential values required to reach $j_{5\ mA\ cm^{-2}}$ for solutions with ethanol at pH ≥ 12, compared to those without ethanol (an average variation of + 0.270 V).

The increased energetic expenditure for the oxidation process can be attributed to the reduction in available Pt-O catalytic sites. This can be rationalized as follows: (*i*) in addition to Pt sites involved in water oxidation (Eq. 5), more metallic Pt sites are regenerated during ethanol oxidation (Eqs. 9 and 12); (*ii*) OH^- ions, required to generate Pt-O groups (Eqs. 6 and 7), must now compete with the strongly adsorbing Cl^- ions, which are present in higher concentrations at the electrode/electrolyte interface due to the enhanced adsorption effect of ethanol molecules; (*iii*) Cl^- ions cannot desorb as ClO^- because this reaction also requires Pt-O moieties (according to the mechanism described in Eq. 13); and (*iv*) as a result, higher potential values must be applied for an appreciable amount of the reactive platinum oxide layer to form and become available [98, 107].

Interestingly, the LSV curves in Fig. 6b show a similar current plateau to that observed for the pure electrolyte solutions. However, this plateau persists at the two higher pH values considered, beyond pH 12. A possible explanation for this could be linked to the inferred increase in Cl^- surface concentration caused by the presence of ethanol. As previously discussed, (*i*) for pH ≥ 12, in the absence of organic species, OH^- ions tend to dominate as the primary reactants in the OER; (*ii*) the addition of ethanol to the medium may induce an increase in Cl^- coverage on the electrode surface, thereby increasing the density of negative charges; and (*iii*) since OH^- ions are also negatively charged, they are expected to experience stronger repulsion when approaching the electrode surface compared to neutral water molecules under the same potential. Consequently, under these assumptions, a higher OH^- concentration (i.e., a higher pH) is naturally expected to be required for the OER to become less competitive relative to the COR.

From an economic perspective, neither the hypochlorous acid/hypochlorite ions formed in the solution with nominal pH between 8 and 11 (Equations S9 and 14) [108], nor the small amounts of acetaldehyde and acetate produced at pH ≥ 12 through this electrochemical process, are commercially competitive compared to existing production methods supplying the global market.

Recently, two chemical products formed by the reaction of ethanol with electrochemically generated active chlorine species in chloride-containing solutions have gleaned attention due to their strategic value in producing higher-value compounds: 2-chloroethanol (a precursor to ethylene oxide) [109] and ethyl hypochlorite (a precursor to 1,1-diethoxyethane) [110]. However, these reactions require specific conditions that are difficult to achieve in the system studied here.

For example, 2-chloroethanol formation requires the chlorine radical (Cl·), generated from a chloride-rich solution using a boron-doped diamond electrode [109]—a material still too expensive for large-scale use. Although the platinum electrode in this study may theoretically form Pt-Cl species, the pH range of 8 to 14 and the predominantly aqueous electrolyte favor Pt-O species, resulting in reactions driven by oxygenated rather than chlorinated intermediates.

Similarly, ethyl hypochlorite formation has been reported through the reaction of ethanol with active chlorine species (still unidentified) on an electrode surface in an anhydrous ethanol solution containing chloride ions from organic salts like tetra-n-butylammonium chloride [110]. Such systems show a characteristic Tafel slope of about 170 mV dec^{-1}, which deviates significantly from those observed in this study. This difference in electrochemical behavior suggests that ethyl hypochlorite formation is unlikely under the aqueous conditions and pH ranges explored here.

Technical challenges and opportunities

In this study of ethanol electro-oxidation in seawater-like environments, several technical challenges emerged that are crucial for optimizing experimental methodologies and gaining a deeper understanding of the system's mechanistic aspects. Addressing these challenges would not only improve the accuracy of the results but also open significant opportunities for advancing the field. Below, we discuss three key areas identified—ECSA determination, crystallographic face identification and control, and interfacial pH monitoring—as well as the expected role

that some promising developments in in situ spectroscopic techniques may play in effectively tackling them.

Accurate determination of electrochemically active surface area

As previously noted, accurate determination of the Electrochemically Active Surface Area is essential for comparing current densities across different experimental conditions. Variations at the electrode/solution interface can significantly alter the system's electrochemical behavior, making precise ECSA quantification critical.

The method employed in this study, based on hydrogen adsorption/desorption, is commonly used for noble metal electrodes. However, as discussed in Section S.1 of the Online Resource, the method's reliability in chloride-rich and pH-variable environments is limited. Additionally, alternative techniques, such as CO stripping voltammetry, were also deemed unsuitable due to the competitive adsorption of chloride ions and ethanol, while capacitive methods posed challenges due to variability in specific capacitance across different pH conditions.

Given these limitations, developing new in situ techniques and methodologies capable of determining the electroactive surface area for a given species in the presence of interface heterogeneities is of paramount importance. In systems like the one discussed here, specific species may block electrode surface sites at lower potentials but become reactive at higher potentials, competing for the same active sites. This dynamic complicates ECSA measurement, particularly when both species interact with the electrode surface simultaneously.

Among the methods considered, using an inner-sphere electron transfer redox probe which with selective adsorption over the metallic sites (e.g., O_2 [111]), combined with the Randles-Sevcik equation, offers a promising approach [112]. However, this method hinges on identifying or synthesizing a compound with the following properties: (*i*) well-defined redox processes that are minimally influenced by ligand structure or composition changes (in coordination compounds) induced by pH variations; (*ii*) resistance to decomposition over a broad pH range, temperature, and electrolyte composition (including ligand exchange or elimination reactions in coordination complexes); (*iii*) low molecular/ionic volume to avoid steric hindrance that could lead to underestimation of the electroactive surface area; and (*iv*) adequate affinity for metallic sites on the electrode surface, but weak enough to allow for easy removal, enabling subsequent electrochemical measurements without requiring aggressive cleaning methods that may alter the ECSA previously measured.

These methodological improvements would enhance the accuracy of ECSA measurements, particularly in complex environments rich in chloride ions and exhibiting variable pH. Future research could focus on refining this approach and identifying suitable redox probes, ultimately enabling more reliable ECSA determinations in these challenging systems.

Identifying and controlling crystallographic face exposure in polycrystalline electrodes

As discussed earlier, selective exposure of crystallographic planes in polycrystalline platinum electrodes is pivotal to optimizing catalytic performance in ethanol electro-oxidation.

In this study, we observed a trend where specific crystallographic faces seem to become preferentially exposed as the pH increases—a phenomenon attributed to variations in adsorption energies across crystallographic faces—with the higher hydroxide concentration favoring the displacement of adsorbed chloride ions.

Manipulating the exposure of crystallographic faces offers significant potential for enhancing catalytic efficiency. By favoring surface orientations that promote desired reactions, one could improve both selectivity and performance in electrochemical processes. This is particularly relevant for large-scale applications, such as seawater desalination and CO_2 capture, where optimizing electrode surface properties could lead to substantial performance improvements.

Although single-crystal electrodes are not feasible for large-scale production, understanding the principles governing crystallographic face exposure in polycrystalline materials could provide a practical alternative. Additionally, exploring more abundant and cost-effective materials, such as nickel and copper—which may exhibit similar face-dependent behavior and even a different adsorption strength order with chloride from that established for platinum ($\{111\} > \{100\} > \{110\}$)—could open new avenues for research in this area.

Nevertheless, for such exploration to be feasible, the challenges associated with the fast and simple identification of crystallographic features under experimental conditions need to be addressed. Currently, the most promising approaches are likely the direct mapping of domain grains on the electrode surface using scanning electrochemical cell microscopy (SECCM) by measuring and comparing the local PZCs with the specific values associated with each crystallographic face (quantitative) [113], and the deconvolution of the electrode's cyclic voltammetric features using fitting functions, such as Lorentzian peaks (qualitative) [114].

However, both of these methods share the same current limitation: the PZC values and the positions and attribution of the voltammetric peaks depend not only on the identity of the crystallographic planes exposed, but also on the pH and

ionic composition of the medium [115–118]. While studies such as those by Xue et al. [119] and McCrum et al. [120] have established very accurate standards for such comparisons for many of the main lower-index Miller surfaces, they did so only for the primary pH values typically considered in the literature (pH 1 and pH 13) and only for media containing 0.1 M of OH^- or ClO_4^- as the sole anions present in solution.

Since it has been shown that even perchlorate anions tend to exhibit a non-negligible degree of adsorption on platinum single crystals—sufficient to affect their characteristic voltammetric peaks [121]—future work with seawater-like solutions would benefit from acquiring such standard values for the main facets of different polycrystalline metallic materials of interest, specifically for solutions containing Cl^- ion concentrations as high as 0.5 M and across a wider range of pH values.

Monitoring interfacial pH variations

In electrochemical systems that lack strong buffering capacity, significant pH variations can occur at the electrode/solution interface during reactions, which can dramatically impact the reactivity and stability of both the electrode surface and the reactive species involved [122]. Monitoring these interfacial pH changes in real time is crucial for optimizing processes like ethanol electro-oxidation in seawater-like electrolytes.

Current methods for tracking interfacial pH, such as using a rotating ring-disk electrode (RRDE) system, present challenges. These methods rely on the reaction of interest occurring on the disk, with the pH change calculated based on the shift in potential required to achieve a given current density on the ring associated with the HER [61, 123]—relative to the standard value determined at the same rotation speed of the electrode in the absence of the disk reaction—or through the use of other specific reactions on the ring for this purpose [124]. However, rotating the electrode alters mass transport and consequently affects the kinetics of reactions generating or consuming H^+/OH^- ions [125]. Additionally, even if the distance between the disk and ring is minimized in such a setup to enable more precise detection of these species based solely on their self-diffusion, this often introduces electronic coupling issues due to the significant overlap of their electric fields, further complicating the process.

Developing precise methods for real-time pH monitoring under static hydrodynamic conditions could lead to significant advancements in controlling the electrochemical environment, particularly in natural waters or seawater-like solutions. Some methods, such as those based on open circuit potential decay transients [126], are being developed and refined, but their use is still far from becoming common practice. This is essential for reactions involving pH-sensitive species such as Cl_2, HClO, or ClO^-, which play key roles in the reactivity of the system. Improved monitoring and control of pH shifts would enhance the selectivity and efficiency of reactions such as organic molecule chlorination or chlorohydrin formation [127–130].

Optimizing the organic/water solvent ratio for electrochemical processes

As previously discussed, the formation of ethyl hypochlorite tends to occur in solutions where ethanol is the primary solvent, but not when ethanol is present in lower concentrations in predominantly aqueous environments [110]. While the ability of a neat ethanol medium to form various active chlorine species and stabilize them long enough to react with its molecules is highly desirable, studies such as those by Mukouyama et al. [131] have demonstrated that the interaction of ethanol with the electrode surface and its derived species, by itself, differs considerably from the reactions typically observed in aqueous media—even forming products through C_3 and C_4 mechanistic pathways.

However, electrochemical reactions in organic media pose significant challenges for large-scale implementation, such as the need for unconventional electrodes and electrolytes. Nevertheless, exploring mixed organic/aqueous solvent systems may offer a promising pathway to optimizing ethanol electro-oxidation in seawater-like environments, potentially accessing reaction mechanisms observed in purely organic systems.

A promising but underexplored avenue could be to increase the ethanol-to-water ratio to levels that allow the use of seawater and its electrolytes, without causing salt precipitation due to the increasing apolarity of the medium. For instance, a 50% molar ratio of ethanol to water could be viable for seawater-derived solutions depleted of divalent cations. This approach would allow investigation into whether the mechanisms observed in purely organic systems could be replicated under more practical working conditions.

Such research could unveil new pathways to improve the selectivity and efficiency of ethanol electro-oxidation, balancing the favorable interactions of organic solvents with the practicality of seawater-like environments. This would significantly broaden the applicability of electrochemical processes for CO_2 mitigation and related technologies.

The importance of advancing in situ spectroscopic techniques

Spectroscopic techniques have long played a pivotal role in investigating electrode/solution interface structures and phenomena, being applied—directly or indirectly, to some extent—to study many aspects related to the challenges

outlined here [132]. However, limitations in spatial and temporal resolution, and the inability of many established protocols to be applied in situ, still hinder their integration into processes requiring fine, near-instantaneous control of multiple variables.

These limitations contribute to the ongoing debate over whether the Pt-OCl species (bound by the oxygen atom) discussed here can directly desorb from the electrode surface as hypochlorous acid or hypochlorite ion, and if that is the case, whether it is the only intermediate capable of this under purely electrochemical conditions [133, 134].

For instance, the following mechanism—adapted from the one proposed by Erenburg, Krishtalik, and Yaroshevskaya in 1975—was one of the earliest attempts to rationalize this process [135]:

$$Pt + Cl^- \rightarrow Pt - Cl + e^- \quad (15)$$

$$Pt - Cl + H_2O \rightarrow Pt - ClOH + H^+ + e^- \quad (16)$$

$$Pt - ClOH + H^2O \rightarrow Pt - OH + H^+ + HClO \quad (17)$$

They considered the discharge of water molecules as the rate-limiting step (Eq. 16). However, they also assumed that the kinetics of the chlorine oxidation reaction would be independent of pH. This assumption regarding the pH-independence of the COR was soon found to be incorrect [136]. As a result, this mechanism largely faded from academic discussions, superseded by more refined models, such as those presented earlier in Eqs. 13 and 14.

Nevertheless, as no further effort was made to confirm the formation of Pt-ClO species (bound by the chlorine atom), it remains difficult to rule out their formation as a possible intermediate under atypical COR conditions, where the adsorption dynamics of Cl^- and OH^-/H_2O are influenced by the presence of a competing species, such as ethanol molecules.

In this context, non-linear optical techniques, such as sum frequency generation (SFG) spectroscopy, hold significant promise. SFG is highly selective for species present at the interface compared to those in the bulk solution, making it particularly useful for identifying adsorbed species [137, 138]. The increasingly common application of pico- and femtosecond pulsed lasers in SFG has been enabling the easier and more precise identification of short-lived surface-bound intermediates, specific sites of adsorption, and even the reorientation dynamics of species on the electrode surface [139–141].

Despite these advantages, the high cost and size of equipment required for SFG measurements remain barriers to widespread application. However, recent advances in optical fiber technology are reducing these costs, making SFG a more feasible option for in situ analysis in the near future [142].

Altogether, these comments suggest promising routes to overcoming current challenges in the field and, if successfully addressed, could potentially offer the level of real-time in situ monitoring and control necessary to further develop ethanol electro-oxidation and related processes in seawater-like environments. By integrating such advances, future research could substantially improve our understanding and management of these complex electrochemical systems.

Conclusions

This study provides relevant insights into the electro-oxidation of ethanol in seawater-like electrolytes, emphasizing the significant influence of pH on the reaction kinetics and chloride ion adsorption on polycrystalline platinum electrodes. Our findings indicate that ethanol oxidation becomes more favorable at higher pH levels, particularly from pH 12 onwards, where reduced chloride adsorption and increased OH^- availability enhance current densities. These observations underscore the potential of alkaline conditions to mitigate surface inhibition caused by chloride ions.

One of the most intriguing outcomes of this work is the observation of dynamic instabilities at pH values above 12, particularly at pH 13, where potential oscillations suggest preferential exposure of specific platinum crystallographic faces—a phenomenon supported by voltammetric trends.

Based on these findings, several hypotheses have emerged, including the modulation of chloride ion distribution on platinum electrode surfaces and the competitive adsorption of ethanol, chloride, and hydroxide ions at higher pH levels. While these inferences provide a plausible explanation of the observed phenomena, further experimental verification using advanced surface characterization techniques is necessary.

Despite the progress made, technical challenges remain, particularly in determining the electrochemically active surface area in chloride-rich environments and addressing mass transport limitations at higher scan rates. Additionally, developing reliable, real-time techniques for monitoring interfacial pH and species identification is crucial for advancing the understanding of ethanol oxidation mechanisms under complex electrolyte conditions.

Ultimately, while challenges remain, this study lays the foundation for further exploration of ethanol electro-oxidation and related reactions in seawater-like electrolytes. It provides critical insights into the technical and mechanistic aspects of the system, potentially paving the way for future advancements in electrochemical CO_2 capture and

mitigation technologies economically assisted by hybrid seawater electrolysis.

Supplementary Information The online version contains supplementary material available at https://doi.org/10.1007/s10008-025-06212-5.

Author contribution Thiago Barros Ferraz: methodology, investigation, formal analysis, validation, visualization, writing—original draft. Germano Tremiliosi-Filho: writing—review and editing. Hamilton Varela: conceptualization, funding acquisition, project administration, supervision, writing—review and editing.

Funding The authors would like to express their thankfulness for the financial support provided to this research by all the funding agencies involved, with special regard to the RCGI–Research Centre for Greenhouse Gas Innovation, hosted by the University of São Paulo (USP) and sponsored by FAPESP–São Paulo Research Foundation (2014/50279-4 and 2020/15230-5) and Shell Brasil. The strategic importance of the support given by ANP (Brazil's National Oil, Natural Gas and Biofuels Agency) through the R&D levy regulation is also acknowledged. The identification codes of the grants in question are listed as follows: Thiago Barros Ferraz: FAPESP (#2021/13002-8) and CNPQ (#140210/2022-9), Hamilton Varela: FAPESP (#2019/22183-6 and #2020/15230-5), Shell Brasil, and CNPq (#311419/2023-2).

Data availability All the experimental data collected and used to draw the conclusions presented here are contained in the text. Further information can be provided upon request via email to the corresponding author.

Declarations

Conflict of interest The authors declare no competing interests.

References

1. Committee on Developing a Research Agenda for Carbon Dioxide Removal and Reliable Sequestration, Board on Atmospheric Sciences and Climate, Board on Energy and Environmental Systems et al (2019) Negative emissions technologies and reliable sequestration: a research agenda. National Academies Press, Washington, D.C.
2. Davies PA, Yuan Q, De Richter R (2018) Desalination as a negative emissions technology. Environ Sci: Water Res Technol 4:839–850. https://doi.org/10.1039/C7EW00502D
3. La Plante EC, Simonetti DA, Wang J et al (2021) Saline water-based mineralization pathway for gigatonne-scale CO_2 management. ACS Sustain Chem Eng 9:1073–1089. https://doi.org/10.1021/acssuschemeng.0c08561
4. La Plante EC, Chen X, Bustillos S et al (2023) Electrolytic seawater mineralization and the mass balances that demonstrate carbon dioxide removal. ACS EST Eng 3:955–968. https://doi.org/10.1021/acsestengg.3c00004
5. Zhang P, Huo Y, Wang F et al (2023) Direct electrochemical seawater splitting for green hydrogen and artificial reefs. ACS Appl Energy Mater 6:7636–7642. https://doi.org/10.1021/acsaem.3c01071
6. Ellis LD, Badel AF, Chiang ML et al (2020) Toward electrochemical synthesis of cement—an electrolyzer-based process for decarbonating $CaCO_3$ while producing useful gas streams. Proc Natl Acad Sci USA 117:12584–12591. https://doi.org/10.1073/pnas.1821673116
7. Xie Q, Wan L, Zhang Z, Luo J (2023) Electrochemical transformation of limestone into calcium hydroxide and valuable carbonaceous products for decarbonizing cement production. iScience 26:106015. https://doi.org/10.1016/j.isci.2023.106015
8. Liu H, She Q (2024) Scaling-enhanced scaling during electrodialysis desalination. ACS EST Eng 4:1063–1072. https://doi.org/10.1021/acsestengg.3c00549
9. Aslam S, Rani S, Lal K et al (2023) Electrochemical hydrogen production: sustainable hydrogen economy. Green Chem 25:9543–9573. https://doi.org/10.1039/D3GC02849F
10. Yao J, Yang R, Liu C et al (2024) Alkynes electrooxidation to α, α-dichloroketones in seawater with natural chlorine participation via competitive reaction inhibition and tip-enhanced reagent concentration. ACS Cent Sci 10:155–162. https://doi.org/10.1021/acscentsci.3c01277
11. Yu Z, Liu L (2024) Recent advances in hybrid seawater electrolysis for hydrogen production. Adv Mater 36:2308647. https://doi.org/10.1002/adma.202308647
12. Sun H, Xu X, Fei L et al (2024) Electrochemical oxidation of small molecules for energy-saving hydrogen production. Adv Energy Mater 14:2401242. https://doi.org/10.1002/aenm.202401242
13. Chen L, Yu C, Dong J et al (2024) Seawater electrolysis for fuels and chemicals production: fundamentals, achievements, and perspectives. Chem Soc Rev 53:7455–7488. https://doi.org/10.1039/D3CS00822C
14. Sallum LF, Mota-Lima A, Gonzalez ER (2019) Galvano– and Potentio–dynamic studies during ethanol electro-oxidation reaction in acid vs. alkaline media: energy dissipation and blocking nature of potassium. Electrochim Acta 293:247–259. https://doi.org/10.1016/j.electacta.2018.09.118
15. Dewan S, Raciti D, Liu Y et al (2018) Comparative studies of ethanol and ethylene glycol oxidation on platinum electrocatalysts. Top Catal 61:1035–1042. https://doi.org/10.1007/s11244-018-0930-5
16. Egeland-Eriksen T, Hajizadeh A, Sartori S (2021) Hydrogen-based systems for integration of renewable energy in power systems: achievements and perspectives. Int J Hydrogen Energy 46:31963–31983. https://doi.org/10.1016/j.ijhydene.2021.06.218
17. Holade Y, Tuleushova N, Tingry S et al (2020) Recent advances in the electrooxidation of biomass-based organic molecules for energy, chemicals and hydrogen production. Catal Sci Technol 10:3071–3112. https://doi.org/10.1039/C9CY02446H
18. Greetham D, Zaky A, Makanjuola O, Du C (2018) A brief review on bioethanol production using marine biomass, marine microorganism and seawater. Curr Opin Green Sustain Chem 14:53–59. https://doi.org/10.1016/j.cogsc.2018.06.008
19. Zaky AS, Greetham D, Tucker GA, Du C (2018) The establishment of a marine focused biorefinery for bioethanol production using seawater and a novel marine yeast strain. Sci Rep 8:12127. https://doi.org/10.1038/s41598-018-30660-x
20. Gomis V, Saquete MD, García-Cano J (2013) CaSO4 solubility in water–ethanol mixtures in the presence of sodium chloride at 25°C. Application to a reverse osmosis process. Fluid Phase Equilib 360:248–252. https://doi.org/10.1016/j.fluid.2013.09.063
21. Kim M-J, Kim S, Shin S, Kim G (2021) Production of high-purity MgSO4 from seawater desalination brine. Desalination 518:115288. https://doi.org/10.1016/j.desal.2021.115288
22. Na H-R, Kim M-J (2019) Determination of optimal conditions for magnesium recovery process from seawater desalination brine using paper sludge ash, sulfuric acid, and ethanol. DWT 157:324–331. https://doi.org/10.5004/dwt.2019.23791
23. Dickson AG, Goyet C (1994) Handbook of methods for the analysis of the various parameters of the carbon dioxide system

in sea water. Version 2. Oak Ridge National Lab. (ORNL), Oak Ridge, TN (United States)
24. Breiter MW (1963) Voltammetric study of halide ion adsorption on platinum in perchloric acid solutions. Electrochim Acta 8:925–935. https://doi.org/10.1016/0013-4686(62)87047-9
25. Gilman S (1964) Studies of anion adsorption on platinum by the multipulse potentiodynamic (M.p.p.) Method. I. Kinetics of chloride and phosphate adsorption and associated charge at constant potential [1]. J Phys Chem 68:2098–2111. https://doi.org/10.1021/j100790a013
26. Bagotzky VS, Vassilyev YB, Weber J, Pirtskhalava JN (1970) Adsorption of anions on smooth platinum electrodes. J Electroanal Chem Interfacial Electrochem 27:31–46. https://doi.org/10.1016/S0022-0728(70)80200-5
27. Horányi G, Inzelt G (1978) Periodical changes in the adsorption of chloride ions accompanying the potential oscillations produced in the course of galvanostatic electrooxidation. J Electroanal Chem Interfacial Electrochem 87:423–427. https://doi.org/10.1016/S0022-0728(78)80166-1
28. Novak DM, Conway BE (1981) Competitive adsorption and state of charge of halide ions in monolayer oxide film growth processes at Pt anodes. J Chem Soc Faraday Trans 1(77):2341. https://doi.org/10.1039/f19817702341
29. Sobkowski J, Wieckowski A (1973) The influence of halide ions on methanol adsorption and oxidation on a platinized electrode. J Electroanal Chem Interfacial Electrochem 41:373–379. https://doi.org/10.1016/S0022-0728(73)80416-4
30. Snell KD, Keenan AG (1982) Effect of anions and pH on the ethanol electro-oxidation at a platinum electrode. Electrochim Acta 27:1683–1696. https://doi.org/10.1016/0013-4686(82)80164-3
31. Snell KD, Keenan AG (1981) Chloride inhibition of ethanol electrooxidation at a platinum electrode in aqueous acid solution. Electrochim Acta 26:1339–1344. https://doi.org/10.1016/0013-4686(81)85119-5
32. Breiter MW (1964) Voltammetric study of the inhibition of methanol oxidation on platinum by chloride ion in acid solution. Electrochim Acta 9:827–833. https://doi.org/10.1016/0013-4686(64)80068-2
33. Breiter MW (1968) Role of adsorbed species for the anodic methanol oxidation on platinum in acidic electrolytes. Discuss Faraday Soc 45:79. https://doi.org/10.1039/df9684500079
34. Sobkowski J, Franaszczuk K, Dobrowolska K (1992) Effect of anions and pH on the adsorption and oxidation of methanol on a platinum electrode. J Electroanal Chem 330:529–540. https://doi.org/10.1016/0022-0728(92)80329-3
35. Kamath VN, Lal H (1968) Kinetics of anodic oxidation of adsorbed films formed on platinized platinum in methanol, formic acid and carbon dioxide solutions. J Electroanal Chem Interfacial Electrochem 19:249–258. https://doi.org/10.1016/S0022-0728(68)80123-8
36. Kumar A, Buttry DA (2016) Influence of halide ions on anodic oxidation of ethanol on palladium. Electrocatalysis 7:201–206. https://doi.org/10.1007/s12678-015-0298-2
37. Attard GA (2018) A phenomenological theory of electrosorption. J Electroanal Chem 819:481–494. https://doi.org/10.1016/j.jelechem.2017.12.057
38. Tong W, Forster M, Dionigi F et al (2020) Electrolysis of low-grade and saline surface water. Nat Energy 5:367–377. https://doi.org/10.1038/s41560-020-0550-8
39. Zhou Q, Liao L, Zhou H et al (2022) Innovative strategies in design of transition metal-based catalysts for large-current-density alkaline water/seawater electrolysis. Mater Today Phys 26:100727. https://doi.org/10.1016/j.mtphys.2022.100727
40. Dresp S, Dionigi F, Klingenhof M, Strasser P (2019) Direct electrolytic splitting of seawater: opportunities and challenges. ACS Energy Lett 4:933–942. https://doi.org/10.1021/acsenergylett.9b00220
41. Lu J, Li C, Wang H et al (2021) How to get to best oxygen evolution behavior from the electrolysis practice of the seawater. Int J Hydrogen Energy 46:12936–12943. https://doi.org/10.1016/j.ijhydene.2021.01.139
42. Arulmozhi N, Esau D, Van Drunen J, Jerkiewicz G (2018) Design and development of instrumentations for the preparation of platinum single crystals for electrochemistry and electrocatalysis research part 3: final treatment, electrochemical measurements, and recommended laboratory practices. Electrocatalysis 9:113–123. https://doi.org/10.1007/s12678-017-0426-2
43. Gilman S (2014) Rate of adsorption of methanol at a polycrystalline platinum electrode in acid solution. J Electroanal Chem 712:47–54. https://doi.org/10.1016/j.jelechem.2013.10.005
44. Doña Rodríguez JM, Herrera Melián JA, Pérez Peña J (2000) Determination of the real surface area of Pt electrodes by hydrogen adsorption using cyclic voltammetry. J Chem Educ 77:1195. https://doi.org/10.1021/ed077p1195
45. Trasatti S, Petrii OA (1992) Real surface area measurements in electrochemistry. J Electroanal Chem 327:353–376. https://doi.org/10.1016/0022-0728(92)80162-W
46. Wang Y, Zou S, Cai W-B (2015) Recent advances on electrooxidation of ethanol on Pt- and Pd-based catalysts: from reaction mechanisms to catalytic materials. Catalysts 5:1507–1534. https://doi.org/10.3390/catal5031507
47. Han L, Ju H, Xu Y (2012) Ethanol electro-oxidation: cyclic voltammetry, electrochemical impedance spectroscopy and galvanostatic oscillation. Int J Hydrogen Energy 37:15156–15163. https://doi.org/10.1016/j.ijhydene.2012.08.034
48. Strbac S (2011) The effect of pH on oxygen and hydrogen peroxide reduction on polycrystalline Pt electrode. Electrochim Acta 56:1597–1604. https://doi.org/10.1016/j.electacta.2010.10.057
49. Shah AH, Zhang Z, Wan C et al (2024) Platinum surface water orientation dictates hydrogen evolution reaction kinetics in alkaline media. J Am Chem Soc 146:9623–9630. https://doi.org/10.1021/jacs.3c12934
50. Gisbert R, García G, Koper MTM (2010) Adsorption of phosphate species on poly-oriented Pt and Pt(1 1 1) electrodes over a wide range of pH. Electrochim Acta 55:7961–7968. https://doi.org/10.1016/j.electacta.2010.04.009
51. Briega-Martos V, Stojanovski K, Zlatar M et al (2024) pH dependence of noble metals dissolution: platinum. Electrochim Acta 501:144793. https://doi.org/10.1016/j.electacta.2024.144793
52. Busó-Rogero C, Herrero E, Feliu JM (2014) Ethanol oxidation on Pt single-crystal electrodes: surface-structure effects in alkaline medium. ChemPhysChem 15:2019–2028. https://doi.org/10.1002/cphc.201402044
53. Morin M-C, Lamy C, Léger J-M et al (1990) Structural effects in electrocatalysis: oxidation of ethanol on platinum single crystal electrodes. Effect of pH. J Electroanal Chem Interfacial Electrochem 283:287–302. https://doi.org/10.1016/0022-0728(90)87396-2
54. Zhu S, Hu X, Shao M (2017) Impacts of anions on the oxygen reduction reaction kinetics on platinum and palladium surfaces in alkaline solutions. Phys Chem Chem Phys 19:7631–7641. https://doi.org/10.1039/C7CP00404D
55. Liao LW, Li MF, Kang J et al (2013) Electrode reaction induced pH change at the Pt electrode/electrolyte interface and its impact on electrode processes. J Electroanal Chem 688:207–215. https://doi.org/10.1016/j.jelechem.2012.08.031
56. Gamboa-Aldeco ME, Herrero E, Zelenay PS, Wieckowski A (1993) Adsorption of bisulfate anion on a Pt(100) electrode: a comparison with Pt(111) and Pt(poly). J Electroanal Chem 348:451–457. https://doi.org/10.1016/0022-0728(93)80151-7

57. Magnussen OM (2002) Ordered anion adlayers on metal electrode surfaces. Chem Rev 102:679–726. https://doi.org/10.1021/cr000069p
58. Gossenberger F, Roman T, Groß A (2015) Equilibrium coverage of halides on metal electrodes. Surf Sci 631:17–22. https://doi.org/10.1016/j.susc.2014.01.021
59. Lai SCS, Kleijn SEF, Öztürk FTZ et al (2010) Effects of electrolyte pH and composition on the ethanol electro-oxidation reaction. Catal Today 154:92–104. https://doi.org/10.1016/j.cattod.2010.01.060
60. Camara GA, Iwasita T (2005) Parallel pathways of ethanol oxidation: the effect of ethanol concentration. J Electroanal Chem 578:315–321. https://doi.org/10.1016/j.jelechem.2005.01.013
61. Figueiredo MC, Arán-Ais RM, Climent V et al (2015) Evidence of local pH changes during ethanol oxidation at Pt electrodes in alkaline media. ChemElectroChem 2:1254–1258. https://doi.org/10.1002/celc.201500151
62. Rus ED, Wakabayashi RH, Wang H, Abruña HD (2021) Methanol oxidation at platinum in alkaline media: a study of the effects of hydroxide concentration and of mass transport. ChemPhysChem 22:1397–1406. https://doi.org/10.1002/cphc.202100087
63. Ertl G (2008) Reactions at surfaces: from atoms to complexity (Nobel lecture). Angew Chem Int Ed 47:3524–3535. https://doi.org/10.1002/anie.200800480
64. Strasser P, Lübke M, Raspel F et al (1997) Oscillatory instabilities during formic acid oxidation on Pt(100), Pt(110) and Pt(111) under potentiostatic control. I. Experimental. J Chem Phys 107:979–990. https://doi.org/10.1063/1.474450
65. Strasser P, Eiswirth M, Ertl G (1997) Oscillatory instabilities during formic acid oxidation on Pt(100), Pt(110) and Pt(111) under potentiostatic control. II. Model calculations. J Chem Phys 107:991–1003. https://doi.org/10.1063/1.474451
66. Lee J, Eickes C, Eiswirth M, Ertl G (2002) Electrochemical oscillations in the methanol oxidation on Pt. Electrochim Acta 47:2297–2301. https://doi.org/10.1016/S0013-4686(02)00075-0
67. Strasser P, Eiswirth M, Koper MTM (1999) Mechanistic classification of electrochemical oscillators — an operational experimental strategy. J Electroanal Chem 478:50–66. https://doi.org/10.1016/S0022-0728(99)00412-X
68. Wolf W, Lübke M, Koper MTM et al (1995) Experimental and theoretical description of potentiostatic current oscillations during H2 oxidation. J Electroanal Chem 399:185–196. https://doi.org/10.1016/0022-0728(95)04275-X
69. Koper MTM (1992) The theory of electrochemical instabilities. Electrochim Acta 37:1771–1778. https://doi.org/10.1016/0013-4686(92)85080-5
70. Koper MTM (1998) Non-linear phenomena in electrochemical systems. Faraday Trans 94:1369–1378. https://doi.org/10.1039/a708897c
71. Kikuchi M, Mukouyama Y, Okamoto H (2008) Chloride ion influencing potential oscillation generated by formaldehyde oxidation. Electrochim Acta 53:7817–7824. https://doi.org/10.1016/j.electacta.2008.05.056
72. Malkhandi S, Bauer PR, Bonnefont A, Krischer K (2013) Mechanistic aspects of oscillations during CO electrooxidation on Pt in the presence of anions: experiments and simulations. Catal Today 202:144–153. https://doi.org/10.1016/j.cattod.2012.05.018
73. Mukouyama Y, Yonezawa S, Taguchi R et al (2014) Regeneration oscillation observed during oxidation of methanol, formic acid, and formaldehyde with chloride ions. Electrochemistry 82:960–965. https://doi.org/10.5796/electrochemistry.82.960
74. Fiori IA, Melle GB, Sitta E (2020) Halide adsorption effect on methanol electro-oxidation reaction studied by dynamic instabilities. J Electroanal Chem 856:113657. https://doi.org/10.1016/j.jelechem.2019.113657
75. Nagao R, Epstein IR, Gonzalez ER, Varela H (2008) Temperature (over)compensation in an oscillatory surface reaction. J Phys Chem A 112:4617–4624. https://doi.org/10.1021/jp801361j
76. Körös E (1974) Monomolecular treatment of chemical oscillation. Nature 251:703–704. https://doi.org/10.1038/251703a0
77. Aller Pellitero M, Álvarez Lamsfus C, Borge J (2013) The Belousov-Zhabotinskii reaction: improving the oregonator model with the Arrhenius equation. J Chem Educ 90:82–89. https://doi.org/10.1021/ed300227w
78. Marin GB, Yablonsky GS, Constales D (2019) Linear and nonlinear relaxation: stability. Kinetics of chemical reactions: decoding complexity. Wiley, pp 169–202
79. Orlik M (2017) Introduction to the dynamic self-organization of chemical systems: part I: basic concepts and techniques of nonlinear dynamics in chemistry. ChemTexts 3:12. https://doi.org/10.1007/s40828-017-0049-5
80. Silva MF, Delmonde MVF, Batista BC et al (2019) Oscillatory electro-oxidation of ethanol on platinum studied by in situ ATR-SEIRAS. Electrochim Acta 293:166–173. https://doi.org/10.1016/j.electacta.2018.10.019
81. Joo J, Uchida T, Cuesta A et al (2013) Importance of acid–base equilibrium in electrocatalytic oxidation of formic acid on platinum. J Am Chem Soc 135:9991–9994. https://doi.org/10.1021/ja403578s
82. Sallum LF, Gonzalez ER, Feliu JM (2016) Potential oscillations during electro-oxidation of ethanol on platinum in alkaline media: the role of surface sites. Electrochem Commun 72:83–86. https://doi.org/10.1016/j.elecom.2016.09.005
83. Previdello BAF, Fernández PS, Tremiliosi-Filho G, Varela H (2018) Probing the surface fine structure through electrochemical oscillations. Phys Chem Chem Phys 20:5674–5682. https://doi.org/10.1039/C7CP08028J
84. Busó-Rogero C, Solla-Gullón J, Vidal-Iglesias FJ et al (2016) Oxidation of ethanol on platinum nanoparticles: surface structure and aggregation effects in alkaline medium. J Solid State Electrochem 20:1095–1106. https://doi.org/10.1007/s10008-015-2970-0
85. Fawcett WR, Filho RCR, Doubova LM (1991) Double-layer studies in ethanolic solutions. Part 1. —Structure of the mercury/ethanol interface in the absence of specific adsorption. J Chem Soc Faraday Trans 87:2967–2970. https://doi.org/10.1039/FT9918702967
86. Wang X, Liu K, Wu J (2021) Demystifying the Stern layer at a metal–electrolyte interface: local dielectric constant, specific ion adsorption, and partial charge transfer. J Chem Phys 154:124701. https://doi.org/10.1063/5.0043963
87. Damaskin B, Palm U, Petyärv E, Salve M (1973) Adsorption isotherm of ions on electrodes for solutions with constant ionic strength. J Electroanal Chem Interfacial Electrochem 47:127–136. https://doi.org/10.1016/S0022-0728(73)80352-3
88. You X, Han J, Del Colle V et al (2023) Relationship between oxide identity and electrocatalytic activity of platinum for ethanol electrooxidation in perchlorate acidic solution. Commun Chem 6:101. https://doi.org/10.1038/s42004-023-00908-3
89. Nishimoto T, Shinagawa T, Naito T, Takanabe K (2020) Microkinetic assessment of electrocatalytic oxygen evolution reaction over iridium oxide in unbuffered conditions. J Catal 391:435–445. https://doi.org/10.1016/j.jcat.2020.09.007
90. Dai L, Qin Q, Zhao X et al (2016) Electrochemical partial reforming of ethanol into ethyl acetate using ultrathin Co_3O_4 nanosheets as a highly selective anode catalyst. ACS Cent Sci 2:538–544. https://doi.org/10.1021/acscentsci.6b00164
91. Idriss H, Seebauer EG (2000) Reactions of ethanol over metal oxides. J Mol Catal A: Chem 152:201–212. https://doi.org/10.1016/S1381-1169(99)00297-6
92. You X, Xu Y, Han J et al (2023) Effect of adsorbed sulfate on the product selectivity of ethanol oxidation on Pt nanoparticles

in acidic solution. J Phys Chem C 127:5743–5753. https://doi.org/10.1021/acs.jpcc.2c08881
93. Zhensheng J, Chanjuan X, Qingmei Z et al (2003) Catalytic behavior of nanoparticle α-PtO2 for ethanol oxidation. J Mol Catal A: Chem 191:61–66. https://doi.org/10.1016/S1381-1169(02)00029-8
94. Asokan K, Krishnan V (1988) Electrochemical oxidation Of ethanol at platinum oxide coated titanium anode. Bull Electrochem 04:369–374
95. Rodríguez JF, Nava JL (2024) Active chlorine electrosynthesis from dilute chloride solutions in a flow cell equipped with a TilTi-Ru-Ir-oxides anode. Chem Eng Process - Process Intensif 196:109634. https://doi.org/10.1016/j.cep.2023.109634
96. Vos JG, Koper MTM (2018) Measurement of competition between oxygen evolution and chlorine evolution using rotating ring-disk electrode voltammetry. J Electroanal Chem 819:260–268. https://doi.org/10.1016/j.jelechem.2017.10.058
97. Batista BC, Sitta E, Eiswirth M, Varela H (2008) Autocatalysis in the open circuit interaction of alcohol molecules with oxidized Pt surfaces. Phys Chem Chem Phys 10:6686. https://doi.org/10.1039/b811787j
98. Sitta E, Varela H (2008) On the open-circuit interaction between methanol and oxidized platinum electrodes. J Solid State Electrochem 12:559–567. https://doi.org/10.1007/s10008-007-0349-6
99. Exner KS (2020) Beyond thermodynamic-based material-screening concepts: kinetic scaling relations exemplified by the chlorine evolution reaction over transition-metal oxides. Electrochim Acta 334:135555. https://doi.org/10.1016/j.electacta.2019.135555
100. Exner KS (2019) Controlling stability and selectivity in the competing chlorine and oxygen evolution reaction over transition metal oxide electrodes. ChemElectroChem 6:3401–3409. https://doi.org/10.1002/celc.201900834
101. Fujita W, Yamaguchi M, Tanaka S, Nakayama M (2023) Rotating ring-disk electrode voltammetry for determining the COR–OER selectivity in seawater electrolysis under neutral to alkaline conditions. J Electrochem Soc 170:036507. https://doi.org/10.1149/1945-7111/acc13c
102. Katsounaros I, Meier JC, Klemm SO et al (2011) The effective surface pH during reactions at the solid–liquid interface. Electrochem Commun 13:634–637. https://doi.org/10.1016/j.elecom.2011.03.032
103. Shinagawa T, Garcia-Esparza AT, Takanabe K (2015) Insight on Tafel slopes from a microkinetic analysis of aqueous electrocatalysis for energy conversion. Sci Rep 5:13801. https://doi.org/10.1038/srep13801
104. McCrory CCL, Jung S, Peters JC, Jaramillo TF (2013) Benchmarking heterogeneous electrocatalysts for the oxygen evolution reaction. J Am Chem Soc 135:16977–16987. https://doi.org/10.1021/ja407115p
105. Zhao X, Ren H, Luo L (2019) Gas bubbles in electrochemical gas evolution reactions. Langmuir 35:5392–5408. https://doi.org/10.1021/acs.langmuir.9b00119
106. Shinagawa T, Ng MT, Takanabe K (2017) Electrolyte engineering towards efficient water splitting at mild pH. ChemSusChem 10:4155–4162. https://doi.org/10.1002/cssc.201701266
107. Santiago PVB, Oliveira RAG, Roquetto JM et al (2019) Oxide formation as probe to investigate the competition between water and alcohol molecules for OH species adsorbed on platinum. Electrochim Acta 317:694–700. https://doi.org/10.1016/j.electacta.2019.06.037
108. Amikam G, Nativ P, Gendel Y (2018) Chlorine-free alkaline seawater electrolysis for hydrogen production. Int J Hydrogen Energy 43:6504–6514. https://doi.org/10.1016/j.ijhydene.2018.02.082
109. Lucky C, Wang T, Schreier M (2022) Electrochemical ethylene oxide synthesis from ethanol. ACS Energy Lett 7:1316–1321. https://doi.org/10.1021/acsenergylett.2c00265
110. Li S, Bartlett BM (2021) Selective chloride-mediated neat ethanol oxidation to 1,1-diethoxyethane via an electrochemically generated ethyl hypochlorite intermediate. J Am Chem Soc 143:15907–15911. https://doi.org/10.1021/jacs.1c05976
111. Ramaswamy N, Mukerjee S (2011) Influence of inner- and outer-sphere electron transfer mechanisms during electrocatalysis of oxygen reduction in alkaline media. J Phys Chem C 115:18015–18026. https://doi.org/10.1021/jp204680p
112. García-Miranda Ferrari A, Foster CW, Kelly PJ et al (2018) Determination of the electrochemical area of screen-printed electrochemical sensing platforms. Biosensors 8:53. https://doi.org/10.3390/bios8020053
113. Wang Y, Gordon E, Ren H (2020) Mapping the potential of zero charge and electrocatalytic activity of metal–electrolyte interface via a grain-by-grain approach. Anal Chem 92:2859–2865. https://doi.org/10.1021/acs.analchem.9b05502
114. Solla-Gullón J, Rodríguez P, Herrero E et al (2008) Surface characterization of platinum electrodes. Phys Chem Chem Phys 10:1359–1373. https://doi.org/10.1039/B709809J
115. Doblhoff-Dier K, Koper MTM (2023) Electric double layer of Pt(111): known unknowns and unknown knowns. Curr Opin Electrochem 39:101258. https://doi.org/10.1016/j.coelec.2023.101258
116. Rizo R, Herrero E, Climent V, Feliu JM (2023) On the nature of adsorbed species on platinum single-crystal electrodes. Curr Opin Electrochem 38:101240. https://doi.org/10.1016/j.coelec.2023.101240
117. Fröhlich NL, Eggebeen JJJ, Koper MTM (2024) Measurement of the double-layer capacitance of Pt(111) in acidic conditions near the potential of zero charge. Electrochim Acta 494:144456. https://doi.org/10.1016/j.electacta.2024.144456
118. Huang J (2022) Surface charging behaviors of electrocatalytic interfaces with partially charged chemisorbates. Curr Opin Electrochem 33:100938. https://doi.org/10.1016/j.coelec.2022.100938
119. Xue S, Chaudhary P, Nouri MR et al (2024) Impact of Pt(hkl) electrode surface structure on the electrical double layer capacitance. J Am Chem Soc 146:3883–3889. https://doi.org/10.1021/jacs.3c11403
120. McCrum IT, Janik MJ (2017) Deconvoluting cyclic voltammograms to accurately calculate Pt electrochemically active surface area. J Phys Chem C 121:6237–6245. https://doi.org/10.1021/acs.jpcc.7b01617
121. Attard GA, Brew A, Hunter K et al (2014) Specific adsorption of perchlorate anions on Pt{hkl} single crystal electrodes. Phys Chem Chem Phys 16:13689–13698. https://doi.org/10.1039/C4CP00564C
122. Lindquist GA, Xu Q, Oener SZ, Boettcher SW (2020) Membrane electrolyzers for impure-water splitting. Joule 4:2549–2561. https://doi.org/10.1016/j.joule.2020.09.020
123. Zimer AM, Medina da Silva M, Machado EG et al (2015) Development of a versatile rotating ring-disc electrode for *in situ* pH measurements. Anal Chim Acta 897:17–23. https://doi.org/10.1016/j.aca.2015.09.047
124. Monteiro MCO, Liu X, Hagedoorn BJL et al (2022) Interfacial pH measurements using a rotating ring-disc electrode with a voltammetric pH sensor. ChemElectroChem 9:e202101223. https://doi.org/10.1002/celc.202101223
125. Seeber R, Zanardi C, Inzelt G (2016) The inherent coupling of charge transfer and mass transport processes: the curious electrochemical reversibility. ChemTexts 2:8. https://doi.org/10.1007/s40828-016-0027-3

126. Sauvé ER, Tang BY, Razdan NK et al (2024) Open circuit potential decay transients quantify interfacial pH swings during high current density hydrogen electrocatalysis. Joule 8:728–745. https://doi.org/10.1016/j.joule.2024.01.004
127. Chung M, Jin K, Zeng JS, Manthiram K (2020) Mechanism of chlorine-mediated electrochemical ethylene oxidation in saline water. ACS Catal 10:14015–14023. https://doi.org/10.1021/acscatal.0c02810
128. Li C-X, Chen C-B, Wang Y-J et al (2019) Insights on the pH-dependent roles of peroxymonosulfate and chlorine ions in phenol oxidative transformation. Chem Eng J 362:570–575. https://doi.org/10.1016/j.cej.2019.01.057
129. Lebedev AT, Shaydullina GM, Sinikova NA, Harchevnikova NV (2004) GC–MS comparison of the behavior of chlorine and sodium hypochlorite towards organic compounds dissolved in water. Water Res 38:3713–3718. https://doi.org/10.1016/j.watres.2004.06.007
130. Deborde M, Von Gunten U (2008) Reactions of chlorine with inorganic and organic compounds during water treatment—kinetics and mechanisms: a critical review. Water Res 42:13–51. https://doi.org/10.1016/j.watres.2007.07.025
131. Mukouyama Y, Iida K, Kuge T (2020) Electrooxidation of ethanol on Pt in the absence of water. Electrochemistry 88:178–184. https://doi.org/10.5796/electrochemistry.19-00056
132. Li C-Y, Tian Z-Q (2024) Sixty years of electrochemical optical spectroscopy: a retrospective. Chem Soc Rev 53:3579–3605. https://doi.org/10.1039/D3CS00734K
133. Zeradjanin AR, Menzel N, Strasser P, Schuhmann W (2012) Role of water in the chlorine evolution reaction at RuO2-based electrodes—understanding electrocatalysis as a resonance phenomenon. Chemsuschem 5:1897–1904. https://doi.org/10.1002/cssc.201200193
134. Luna-Trujillo M, Palma-Goyes R, Vazquez-Arenas J, Manzo-Robledo A (2020) Formation of active chlorine species involving the higher oxide MOx+1 on active Ti/RuO2-IrO2 anodes: a DEMS analysis. J Electroanal Chem 878:114661. https://doi.org/10.1016/j.jelechem.2020.114661
135. Trasatti S (1987) Progress in the understanding of the mechanism of chlorine evolution at oxide electrodes. Electrochim Acta 32:369–382. https://doi.org/10.1016/0013-4686(87)85001-6
136. Evdokimov SV (2000) Mechanism of chlorine evolution-ionization on dimensionally stable anodes. Russ J Electrochem 36:227–230. https://doi.org/10.1007/BF02827964
137. De R, Dietzek-Ivanšić B (2022) A happy get-together – probing electrochemical interfaces by non-linear vibrational spectroscopy. Chem –Eur J 28:e202200407. https://doi.org/10.1002/chem.202200407
138. Han H-L, Horowitz Y, Somorjai GA (2018) A review on in situ sum frequency generation vibrational spectroscopy studies of liquid–solid interfaces in electrochemical systems. Encyclopedia of interfacial chemistry. Elsevier, pp 1–12
139. Zwaschka G, Lapointe F, Campen RK, Tong Y (2021) Characterization of ultrafast processes at metal/solution interfaces: towards femtoelectrochemistry. Curr Opin Electrochem 29:100813. https://doi.org/10.1016/j.coelec.2021.100813
140. Lapointe F, Wolf M, Campen RK, Tong Y (2020) Probing the birth and ultrafast dynamics of hydrated electrons at the gold/liquid water interface via an optoelectronic approach. J Am Chem Soc 142:18619–18627. https://doi.org/10.1021/jacs.0c08289
141. Zwaschka G, Tong Y, Wolf M, Kramer Campen R (2019) Probing the hydrogen evolution reaction and charge transfer on platinum electrodes on femtosecond timescales. ChemElectroChem 6:2675–2682. https://doi.org/10.1002/celc.201900336
142. Liao J, Sun J, Du M, Qin Y (2014) Proposal for sum-frequency generation based on modal phase-matching in photonic crystal fibers. Opt Fiber Technol 20:90–94. https://doi.org/10.1016/j.yofte.2013.12.005